EMI Investigation and Suppression Filter Design for Wireless Robotic Control Applications

Robert Zadeh

A Thesis
in
The Department
of
Electrical and Computer Engineering

Presented in Partial Fulfillment of the Requirements
for the Degree of Master of Applied Science (Electrical Engineering) at
Concordia University
Montréal, Québec, Canada

January 2010

Your file Votre référence
ISBN: 978-0-494-67243-3
Our file Notre référence
ISBN: 978-0-494-67243-3

ABSTRACT

EMI Investigation and Suppression Filter Design for Wireless Robotic Control Applications

Robert Zadeh

This research work contributes to the practical issues of radiated Electromagnetic Interference (EMI) measurements, analysis, and filter design for wireless robotic control. Detailed procedures and hardware setup used for the EMI measurements conducted at the NRC-AMTC factory floor have been presented. Then, the measured radiated EMI levels have been compared to the regulated limits on radiated EMI for Class A industrial equipment. The mentioned radiated EMI level measurements determined the problematic frequencies where the USA Federal Communications Committee (FCC) radiated EMI levels have been exceeded.

The second phase involved band stop filter (BSF) design at the problematic frequencies. Initial filter models were designed using Ansoft Designer, where the characteristic impedance of series and shunt stubs were proposed and calculated by the software. Next, the BSF models were realized using microstrip technology. The dimensions of transmission lines were calculated based on the substrate thickness and the cutoff frequency of interest. BSFs were designed to maximize frequency-selectivity at the cutoff frequencies.

Finally, the built BSF prototypes were built for higher-than-680 MHz models on Rogers RT/duroid® 5880 high-frequency substrates. The S-parameters and phase responses of the BSF prototypes were measured using a network analyzer. The measured results were close to the simulated ones, with an emphasis on selectivity at the cutoff frequencies. BSFs designed at cutoff frequencies of 840 MHz or higher are used while the robot performs arc-welding and peen-forming, while BSFs with cutoff frequencies lower than 840 MHz will be used near the moving-gantry, and while friction stir-welding processes.

Acknowledgements

I would like to express my gratitude towards my supervisor, Dr. Abdel R. Sebak, for his valuable teachings, encouragement, and advice throughout the course of this research work. I would also like to express gratitude towards my former supervisors, Dr. Vijay Devabhaktuni and Dr. Xiaofeng Wang for their financial support and guidance through the preliminary stages of this research project.

I would like to express my appreciation to Dr. Donald Davis (part-time faculty in the ECE department of Concordia) for his advice on EMI measurements and theory. I also like to thank Dr. Iraj Mantegh (my supervisor at the National Research Council Canada-Aerospace Manufacturing Technology Center) for his guidance and encouragement. Dr. Ali Grami (University of Ontario Institute of Technology) is highly appreciated for his invaluable support and positive encouragement. I also like to thank Mr. Jeff Landry (ECE department laboratory technician) for fabricating the filters. In addition, I would like to thank I like to thank my colleagues, Mr. Michael Wong (Ph.D. candidate) and Dr. Alpur Ozturk (post-doctorate research fellow) provided insights to the filter design, fabrication, and testing.

Finally, I like to thank my family and friends for their continuing and unconditional support.

Table of Contents

List of Figures

Chapter 1

Chapter 3

Chapter 4

Chapter 5

List of Tables

Chapter 2

Chapter 3

Chapter 4

List of Acronyms and Symbols

Acronyms

ACSR	Adjacent Channel Selectivity Ratio
ADS	Advanced Design System
BNC	Bayonet Neill-Concelman
BPF	Band Pass Filter
BSF	Band Stop Filter
BW	Bandwidth
CAD	Computer Aided Design
CM	Common Mode
DM	Differential Mode
DPI	Direct Power Injection
DUT	Device Under Test
EM	Electromagnetic
EMC	Electromagnetic Compatibility
EMI	Electromagnetic Interference
EUT	Equipment Under Test
FCC	Federal Communications Commission
HFSS	High Frequency Structure Simulator
IC	Integrated Chip
IL	Insertion Loss
I/O	Input/Output
LISN	Line Impedance Stabilization Network

MATLAB	Matrix Laboratory
MM	Mixed Mode
MMIC	Monolithic Microwave Integrated Circuit
MOS	Metal-Oxide Semiconductor
NRC-AMTC	National Research Council-Aerospace Manufacturing Technology Centre
Op-Amp	Operational Amplifier
PCB	Printed Circuit Board
PLC	Programmable Logic Control
RF	Radio Frequency
RFI	Radio Frequency Interference
RLC	Resistor Inductor Capacitor
RMS	Root Mean Square
SM	Surface Mount
SNR	Signal to Noise Ratio
S-Parameters	Scattering Parameters
UHF	Ultra High Frequency
VHF	Very High Frequency

Symbols

C_P	Shunt Capacitance
dB	Decibels
fc	Cutoff Frequency
f_l	Lower Frequency
f_u	Upper Frequency

Hz	Hertz
L_S	Series Inductor
M	Antenna-Type Parameter
P_{LR}	Power Loss Ratio
Q	Quality Factor
Q_L	Loaded Quality Factor
t	Thickness of the Conductor
t'	Thickness of Dielectric Substrate
W	Width of the Conductor Line
Z_o	Characteristic Impedance
β	Imaginary Phase Constant
δ	Skin Depth of the Metal
Γ	Reflection Coefficient
ε	Electrical Permittivity
ε_{eff}	Effective Permittivity of Dielectric
θ	Angle between Electric Field of the Antenna and the xy-plane
λ	Wavelength
λ_c	Wavelength Calculated at the Cutoff Frequency
σ	Conductivity of the Metal
μ_0	Free Space Magnetic Permeability
φ	Angle between Electric Field of the Antenna and the x-axis
Ω	The Ohms (Unit of Impedance)

Chapter 1

Introduction

1.1 Introduction to Electromagnetic Interference

Electromagnetic Interference (EMI) emanates from electromagnetic conduction, and the radiations of an external noise source that is incident on electronic circuit components. EMI causes unwanted signal degradation, which negatively affects the effective performance of the circuit. The EMI source can be either natural or man-made. Examples of the former include storm and northern lights. Examples of the latter include EMI noise generated by electrical machines, welding equipment, and electrical circuit switch boxes.

In particular, wireless communication systems, multi-purpose electronic circuits, computer motherboards, and many other solid-state devices used on a daily basis are susceptible to various man-made and natural sources of EMI noise. The effects of Electromagnetic Interference (EMI) can be detrimental to the overall performance of any of the above-mentioned devices, if such interference is not controlled or suppressed properly.

Generally, EMI adversely affects the quality of wireless robotic control systems. The measured radiated EMI noise levels in the vicinity of the robotic controller, wireless receiver module, and the wireless network are all crucial in determining the exact design

parameters of the mitigation EMI filter. Such parameters include the pass band, amplitude level of the acceptable signal, filter bandwidth and corner frequencies, filter order, and the insertion loss. The radiated EMI results show deviations from the FCC regulations within the band of data communications.

1.2 Introduction to the Problem

A particularly important wireless performance criterion is its robustness against Electromagnetic Interference (EMI) from various electrical noise sources. It is expressed in decibel with reference to 1μV per meter length of cable (i.e., dBμV/m) at frequency range of *900MHz - 5GHz*. Figure 1 depicts the EMI measurement setup near the robotic controller and its manipulator arm.

The measured radiated EMI in the vicinity of the robotic controller was the milestone of this research project. The details of these measurements are outlined in Chapter 3. Radiated EMI levels were measured and analyzed in the 216-960 MHz and 960-5000 MHz bands. The problematic levels were identified according to the FCC limits on radiated EMI levels of Class A industrial equipment and FCC Class B commercial equipment. This standard dictated the maximum allowed radiated EMI levels at specific frequencies of interest. Then, the next task of this research work included designing and fabricating appropriate band reject filters for the specified problematic frequency ranges of Chapter 3. Chapters 4 and 5 of this thesis will explain the theory, design, and measurement of the band reject filters used for EMI suppression in detail. Tables 3.3 and

3.4 show that the radiated interference is quite larger than the stringent Federal Communications Commission (FCC) standard limits for *Class A Industrial Devices* at operation frequencies past *216 MHz,* as outlined in [1]. Similar EMI measurements were taken near another robot controller, as depicted in Figure1.1. Here, the radiated EMI near the robotic controller is past the *Fail Limit* at frequency bands near *1.9GHz*, according to [1] and [2].

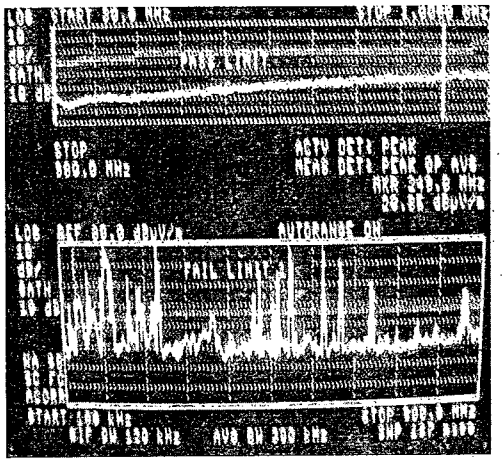

Figure 1.1 Measured Radiated EMI 10 m away from the Motoman® Robotic Controller

The FCC requirements are stringent and the EMI measurement procedures of Chapter 3 adhere to the standards stated in [1] and [3]. This will result the measured signal being in the *Fail Limit* region of the EM analyzer, as shown in Figure 1.1. EMI energy spill results in the deterioration of the wireless interfacing system. A great deal of research and innovation goes into EMI/RFI mitigation and error control in wireless communications. Chapter 3 will cover the details and theoretical background of the EMI measurements for this research project. Figure 1.1 illustrates the typical radiated EMI measured 10 m away from the robotic controller.

1.3 Motivation and Objectives

The above-mentioned EMI results pave the path to the next phase of this work. This research project will first provide a comprehensive study of what has been analyzed, modeled, and designed/proposed for the mitigation of EMI in similar RF and solid-state applications. Moreover, a general summary of the past work will be presented. Then, computer simulation results will be provided on various types of band reject filters for the frequency bands of 216-960 MHz and 960 MHz – 5 GHz.

The main objective is to filter out redundant noise levels above the maximum allowed limits by the FCC Class A and B regulations, while maintaining the required amplitude levels of the original data being sent from the transmitter.

A new range of RF filters will be designed and presented for the mitigation of EMI present in the 216-960 MHz frequency band. The computer simulation results, discussion, and suggestions for further work will also be presented. Next, a similar, yet more frequency-sensitive filter will be designed for the *960MHz – 5GHz* frequency band. The lumped-element models of the proposed filters will be fabricated using lines and stubs on substrates. Further improvements and future work will also be discussed.

1.4 Organization of this Document

This thesis started with this chapter introducing the reader to EMI, motivation behind this research work, thesis objectives, and overview of the document. Chapter 2 of this thesis will address a comprehensive survey of previous work in both EMI/EMC and in RF Filter Design. Details of the conducted EMI measurements at the National Research Council Canada-Aerospace Manufacturing Technology Centre (NRC-AMTC) and the relevant theory will be presented in Chapter 3. The RF filter design methods, circuits, and the simulation results will be presented in Chapter 4. The mentioned filters of Chapter 4 will be fabricated on substrates and tested in Chapter 5. Finally, the thesis will be wrapped up in Chapter 6, where future work in this research topic will also be discussed.

1.5 Summary of Chapter 1

Introduction to the research problem, its significance, and a comprehensive review of the objectives of this research project have been presented in this chapter. A briefing of the proposed filter design, along with the overview of this thesis, has also been provided. Finally, the overall organization of this thesis has been provided.

Chapter 2

Literature Survey of Previous Works

2.1 EMI/EMC and Measurements

The nonlinear model of EMI on both analog and digital communication systems has been presented in [4] and [5]. The mathematical model for the EMI has been presented in the mentioned references. Moreover, the quadrature modeling technique has been presented for the behavioral-level nonlinear modeling and simulation of the active stages of communication circuits and systems. However, no indication or studies of EMI mitigation has been presented.

Analog circuit design techniques for ensuring electromagnetic reliability have been presented in [6]. The optimization techniques have been discussed and verification methods such as EMC simulations, feasibility studies, power crosstalk and simulation of circuit EMI have been demonstrated. The models can be used in the design verification part of this project.

In [7], the detrimental effects of EMI on operational amplifiers and switching capacitors have been presented. An overview of the hazardous electromagnetic environment noises in the frequency band 30-300 Hz has been provided in [7]. Both natural and man-made sources of noise have been introduced. The minimum and maximum noise levels have been demonstrated, with no further suggestions on measurement or mitigation techniques.

A new RFI circuit for MOS switches has been proposed, partially useful in the design stages of this thesis. The double differential pair has been modeled and the prediction of errors due to MOS switch distortion have been mathematically modeled and linked to RFI. Moreover, the RFI-induced errors in complex operational amplifier circuits have been modeled and simulated. A novel EMI filter has been proposed in [8], which is based on the insertion loss method of filter design.

Very comprehensive statistical-physical model of EMI has been presented in [8]. Radiated EMI for Class A and Class B devices have been reproduced, where classification has been conducted based on *a posteriori* probability distribution models. Both intelligent and non-intelligent (man-made and natural) models of noise have been addressed. No indication of measurement or mitigation techniques has been presented. However, the mathematical models described can pave the path to a more realistic realization of the affected network, hence more clear design objectives.

Coupling mechanisms of RF power cords inside an IC have been analyzed and the noise levels have been measured for Direct Power Injection (DPI) circuits and for Operational

Amplifiers (Op-Amps). Then, an analog filter topology has been proposed for the frequency orders of kHz and MHz, which is applicable to IC components and operational amplifiers directly connected to the power injection node. The results on these in addition to the optimized EMI filter will be applied in the design stage of this project, in addition to seeing future improvements to the EMI filter designs.

2.2 EMI/EMC Regulations for Electronic Equipment

In Canada and USA, the limits on radiated EMI on FCC Class A industrial and Class B commercial electronic equipment are regulated by the Federal Communication Commission (FCC). Class A digital electronic devices are those used in commercial, industrial, or business applications. Class B digital electronic devices are used in residential applications, in spite of their application in commercial, industrial, or business environment. The limits on the radiated EMI for FCC Class A equipment measured at 10 m from the noise source have been tabulated in Table 2.1 [1] [9].

Frequency Range (MHz)	**30-88**	**88-216**	**216-960**	**960-5000**
FCC Class A Emission Limits (dBμV/m)	39	43.5	46.4	49.5

Table 2.1 FCC Limits on Class A Emissions at Various Frequency Bands

It is important to note that the limits of Table 2.1 assume a distance of 10 m between the EMI measuring device and the source of radiated EMI. Due to the limitations in the factory floor, safe working distance from the robotic arms and the enclosure of the robotic controller and manipulator arms, all the measurements for this research project are based on a separation distance of 10 m between the EMI analyzer and the noise source.

The standard values of Table 3.3 at the specified frequency ranges will provide proper yardsticks to compare the measured radiated EMI emissions of Chapter 3 against. Simply put, if the measured value of emission at a given frequency exceeds the corresponding limit from Table 3.3, it will be considered unacceptable and must be compensated by appropriate filtering and signal shaping. These regulations are being used as comparison yardsticks in [10] and [11] to evaluate the performance of EMI filter after insertion. Several EMI filters have been proposed in the literature. An active EMI filter for High Frequency (HF) power inverters has been proposed in [10]. This active filter utilized ferrite toroidal core in common mode (CM) to detect high frequencies and leakage currents. Also, the filter leverages a capacitor with high withstand voltage for circuit protection in voltage test conditions. Also, measurement results of the mains terminal interface voltage in [10] show a decrease in CM noise. Theoretical background on EMI measurements before and after filtering, as well as the effects of both the CM and DM radiated EMI noise on the filter have been provided in [10], [11].

2.3 RF Filter Design and Fabrication

The design of a tuned band reject filter has been studied in [12], where the filter is used in the input of power line communication systems. A simple RLC filter has been proposed for "tuned" EMI filtering in conjunction with conventional EMI filtering techniques. The proposed filter has improved the overall results when cascaded with the conventional EMI filter. Also, it has been applied to television receiver and has reduced the overall EMI from adjacent power cords and switches.

A very important application-oriented paper, this thesis will use its techniques in RLC filter design and in proper cascading with the existent filter. As explained in detail in [13], EMI/RFI filter design is still fairly new and lots of research has to go through such projects.

Several design methods have been proposed to model lumped-element filter prototypes on substrates using transmission lines and stubs in [14] and [15]. Simulation results from ADS software can be accordingly compared against these results, due to the accuracy of the ADS software.

In [15], the electromagnetic susceptibility of some typical RF circuits and integrated circuits has been modeled, and the general issues involved in externally-coupled EMC and intra-element EMC have been discussed. From a practical standpoint, the susceptibility of integrated circuits has also been discussed. The parasitic emissions of

ICs, design alternatives to achieve low emission, EMC modeling of some circuit components, and establishing standards in EMC of ICs are relevant to this research work. Filters attenuate the signal magnitude at specific frequencies called "stop band", while permitting signal energy at other frequencies called "pass band".

In most microwave and Radio Frequency (RF) systems, filters are designed and implemented to get rid of spurious signal components and to shape signals. RF filters are traditionally built via waveguides, coaxial lines, and lumped elements. Newer RF filters printed on substrates are lower in cost, have high precision, and are easily implemented into the rest of an electronic system's hardware.

These methods involve filter design by the "insertion loss" method and "image parameter" method. Due to the practicality of the former and the ability to transform lumped element models into transmission lines using mathematical transformations (i.e., Richard's and Kuroda's transformations), the "insertion loss" method has been implemented to design the filters for this research work. Furthermore, electromagnetic simulators such as Ansoft HFSS [16] and RF simulators such as Agilent ADS [17] have been utilized together to design the filter's circuit and translate the design into the transmission lines and stubs.

Determination of the balancing capacitor explained in [11] and the Ultra High Frequency (UHF) filter designed in [18] will prove helpful in the design of EMI filters in Chapter 4 of this thesis. The Mixed Mode (MM) EMI noise have been introduced in [19], where an

RF filter has been design to mitigate the noise by using CM and Differential Mode (DM) chokes.

Details of designing proper band reject filters and their microstrip realizations on dielectric substrates are presented in [19]-[24]. The methods used in the mentioned works have been used in the design and fabrication of the band reject filters for this research work. The design typically starts with the design specifications, cutoff frequency, steepness, and quality factor. The microstrip lines will resemble the corresponding inductance and capacitance values, taking into consideration the thickness of the substrate and the relative dielectric constant of the substrate.

A novel tunable small-size Band Stop Filter (BSF) has been developed for similar aerospace applications and frequencies up to 5 GHz in [25]. This filter uses High Temperature Superconducting film and planar microwave components to achieve insertion loss of -42 dB at f_c = 1.635 GHz. The results of [25] will be used as yardsticks of comparison for the filters of this research work.

Chapters 4 and 5 of this thesis focus on the mentioned filter design methods, application, simulation, and fabrication of several prototypes. These filters will then be used to address the EMI issues of the wireless robotic control system and will pave the ground for further research in this new field of wireless mechatronics and control.

2.4 Simulation Tools and Techniques

Numerous Microwave and RF simulation software tools are available and have been used extensively in most of the surveyed work of this chapter. For this research work, we examined Agilent ADS, Ansoft HFSS, Ansoft Designer, and MATLAB [26]. All the mentioned simulation software tools were analyzed and tested for filter design and fabrication. Parameters such as the simulation time, number of iterations, and the capability of the software to make Gerber files for filter fabrication made up the comparison chart.

In [27], various new Electrical Engineering CAD software such as Ansoft HFSS and ADS have been introduced and compared against for the purpose of EM-based design projects. Ansoft HFSS and Designer have been selected as the simulation tool of choice to verify new design algorithms, and hereby optimizing EM circuit design. Moreover, the BSFs of Chapter 4 were primarily designed in MATLAB before getting re-designed in HFSS due to MATLAB's inability to assist in designing practical microstrip Band Stop Filters (BSFs) and build the corresponding Gerber files as the output.

For this research work, the Ansoft Designer was chosen as the software of choice due to its stability, as well as its fast iterations and effective Gerber file construction capability. Ansoft Designer was also proven to provide very accurate S-parameter analysis and assist in adjusting the dimensions to obtain the best possible performance.

2.5 Summary of Chapter 2

A comprehensive review of previous work on EMI measurements, analysis, and filter design to remedy the issue has been presented in this chapter. Moreover, filter design simulation software have been introduced along with the best choice for this research project. The FCC standards on radiated EMI levels for Class A industrial devices have also been presented, along with some average radiated EMI limits and measurements at frequencies ranging from 300 MHz - 5 GHz.

Chapter 3

Radiated EMI Measurements and Analysis

3.1 Radiated EMI Background

Accurate definition for radiated EMI involves the propagation of electromagnetic energy levels from the EM noise source (the power converter, transmission line, switch, etc.) to the noise victim device, such as the Equipment Under Test (EUT), circuit board, IC, and the robotic controller.

Electromagnetic energy consisting of perpendicular $\vec{E}$ and $\vec{H}$ fields propagating in an array through a medium and negatively affect the performance of radio frequency communications link between the transmitter (modem attached to the supervisory computer) and the receiver (robotic controller).

Electromagnetic energy emanating from an external or an internal source to the electrical equipment negatively affects the neighboring equipment by introducing unwanted and erroneous current components, causing it to have erroneous undesirable response. Typically, signal performance degradation is the by-product of the spurious EMI effect.

EMI usually gets radiated through openings in equipment such as faulty cable shields, holes on the surface of the equipment, or faulty joints in the equipment panels. It is important to remember that metals radiating electromagnetic energy have the capability of absorbing electromagnetic energy. Hence, even an EMI source is vulnerable to EMI from another external source at the same time.

Differential mode and common mode noise are two major radiated noise factors relevant to this research work dealing with radiated noise in electronic equipment. From these two major types, the common mode noise is the main concern, which could make the results of radiated emission become more problematic [28].

The next two sections of this chapter will further elaborate on the two major types of noise, as well as the sources of EMI noise. Then, the details of the measured radiated EMI near the robotic controller and some of the typical noise-contributing equipment will be provided. Finally, the gathered measurements will be analyzed and compared against the FCC limits on radiated EMI.

3.1.1 Differential-Mode and Common-Mode Noise

Differential mode noise is measured between two transmission lines that share a common reference ground. The differential mode noise is formulated as the difference of the noise components of the two transmission lines.

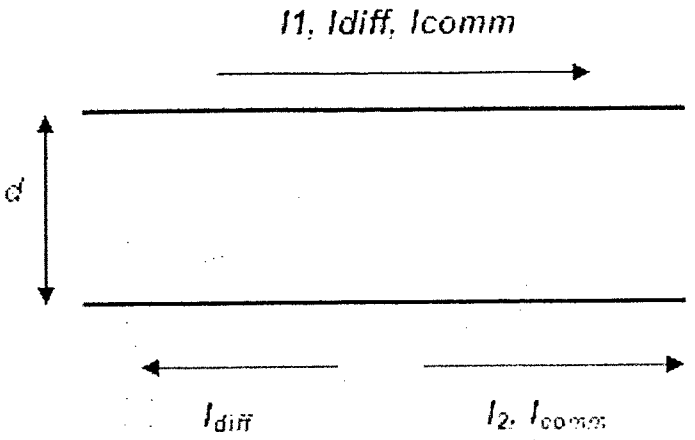

Figure 3.1 Common-Mode and Differential-More Currents of two Parallel Wires

Given two parallel transmission lines of Figure 3.1, with I_1 and I_2 as the currents passing through the wires, the differential mode component of the current can be written as [1]:

$$I_{diff} = \frac{I_1 - I_2}{2} \tag{3.1}$$

, where I_1 and I_2 are the currents through cross section of the wires, along the positive xy-plane direction. Similarly, the ubiquitous and undesired common-mode component of the currents, I_{comm}, can be written as:

$$I_{comm} = \frac{I_1 + I_2}{2} \tag{3.2}$$

One of the most common causes of the differential noise between two transmission lines is the signal to the common loop enclosures alternating magnetic field, which induces voltage in the loop. It is also likely that the alternating electric field terminating on both

signal and common lines to cause currents producing different voltages due to different impedances in the path of each of the currents. The existent noise between the neutral and the ground transmission lines is referred to as the common mode noise. Another way to think of the common mode noise is the coherent interference with a negative effect on two or more elements of a network in a highly-coupled manner.

At higher frequencies, coupling between the conductors, line, neutral and ground will increase. Electronic equipment is typically 10 to 100 times more sensitive to common mode noise [29]. Finally, it is important to note that common-mode currents are very substantial, and often lead to more significant radiated emissions that their differential-mode counterparts, due to the inter-modulation product of currents.

In both cases of differential and common-mode, it is desirable to calculate the total radiated electric field of the wire currents as the sum of each individual one. According to Figure 3.2 [1], the radiated electric field from each of the two wires is:

$$E_{\theta,i} = M I_i \frac{e^{-j\beta_0 r_i}}{r_i} \sin\theta \tag{3.3}$$

, where:

$$M = j\,(2\pi .10^{-7}) f.l \tag{3.4}$$

, where f and l refer to the frequency and line length, respectively.

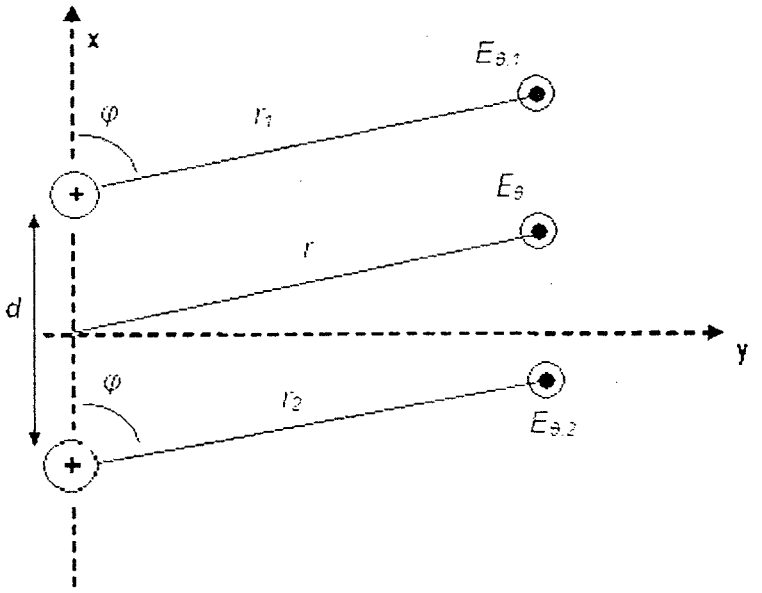

Figure 3.2 Radiated Electric Fields of Parallel Wires

Equations (3.3) and (3.4) refer to the Hertzian dipole as explained in [1]. They are functions of the physical characteristics of the antenna and the angle of the antenna pattern.

As geometrically explained in Figure 3.2, the addition of two current components of two parallel wires will contribute to the total radiated electric field as:

$$E_{\theta,\,tot} = M\,(I_1 \frac{e^{-j\beta_0 r_1}}{r_1} + I_2 \frac{e^{-j\beta_0 r_2}}{r_2}) \tag{3.5}$$

In order to thoroughly understand the difference between the differential and common modes of the noise, equation (3.5) can be re-written for both the mentioned modes

discretely. According to [1], the differential and the common mode components of current can be written as:

$$E_{diff,max} = -4\pi \times 10^{-7} \frac{flI_{diff}}{d} e^{-j\beta_0 d} \sin\left(\frac{1}{2}\beta_0 d\right) \tag{3.6}$$

and

$$E_{comm,max} = -4\pi \times 10^{-7} \frac{flI_{comm}}{d} e^{-j\beta_0 d} \cos\left(\frac{1}{2}\beta_0 d\right) \tag{3.7}$$

, where:

$$r_1 = r - \frac{d}{2} \cos\varphi \tag{3.8}$$

$$r_2 = r + \frac{d}{2} \cos\varphi \tag{3.9}$$

In other words, both differential and common noise components comprise of the same physical parameters, except for their current components. Moreover, a phase shift is present due to the $sin\left(\frac{1}{2}\beta_0 d\right)$ and $cos\left(\frac{1}{2}\beta_0 d\right)$ factors. Next, we shall determine typical sources contributing to the mentioned noise currents in the typical factory floor.

3.1.2 Sources Contributing to Noise

The measured radiated EMI noise levels were conducted near the robotic controllers, friction stir welding machine, transformer box, and the moving robotic gantry. The

frequency range of 300-1800 MHz was particularly of interest since the mentioned equipment showed higher-than-limit quasi-peak radiated EMI levels within this range.

The particular sources of noise involved switching frequency operations in the transformer box, heat generated by high currents of the friction stir welding machine, and the higher-than-normal voltage levels at the robotic controller. Moreover, it was observed during the measurements that the peak radiated EMI noise levels were also adversely affected by operators walking in the vicinity of the log-periodic measurement antenna.

The next section will focus on the EMI measurement setup, equipment, and the formulas and correction factors of the measured EMI levels using the EM analyzer.

3.2 EMI Measurement Equipment Setup

The radiated EMI measurements were conducted using an EM analyzer, log-periodic antenna, 3-meter coaxial cable, and a laptop PC. Figure 3.3 illustrates the typical setup of the mentioned equipment used in conducting the radiated EMI measurements. The basic blueprint of the EMI measurement equipment connections is illustrated in Figure 3.3 (a).

BNC cables of appropriate lengths with cable factors of 1 dB have been used to connect the equipment and the antenna together. The actual equipment used to measure the radiated EMI levels as well as and their connection diagram have been illustrated in Figure 3.3 (b). The directions of the arrows represent the data flow direction in the cables.

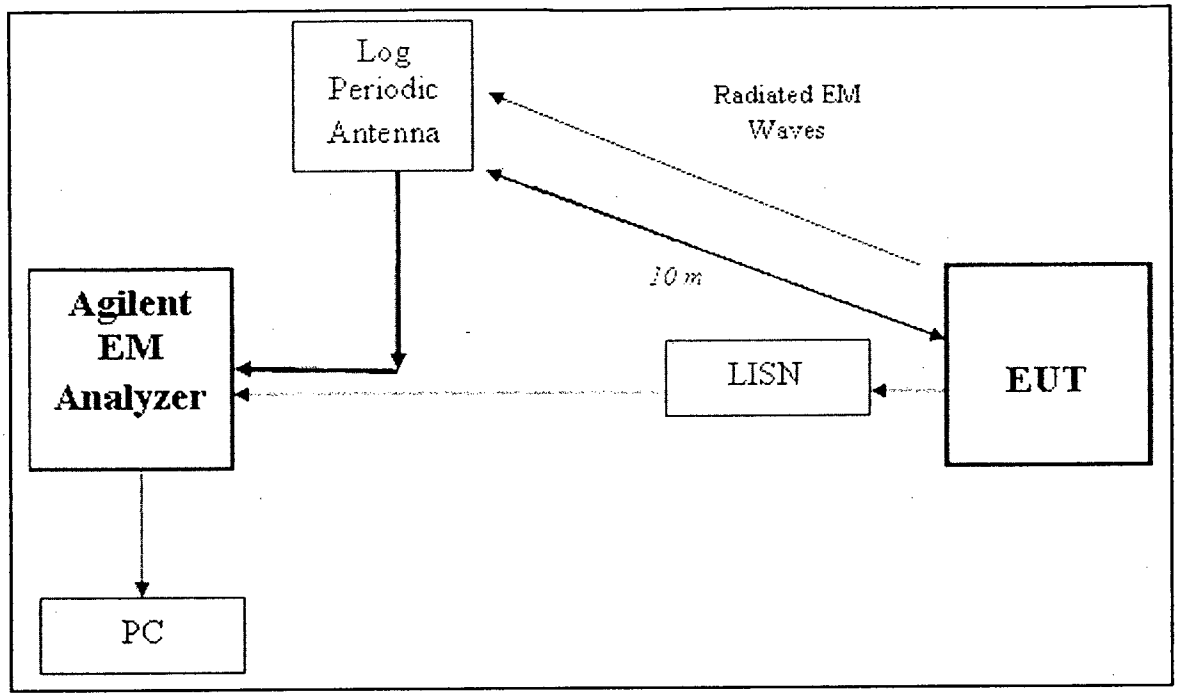

Figure 3.3 (a) Block Diagram of Typical EMI Test Equipment

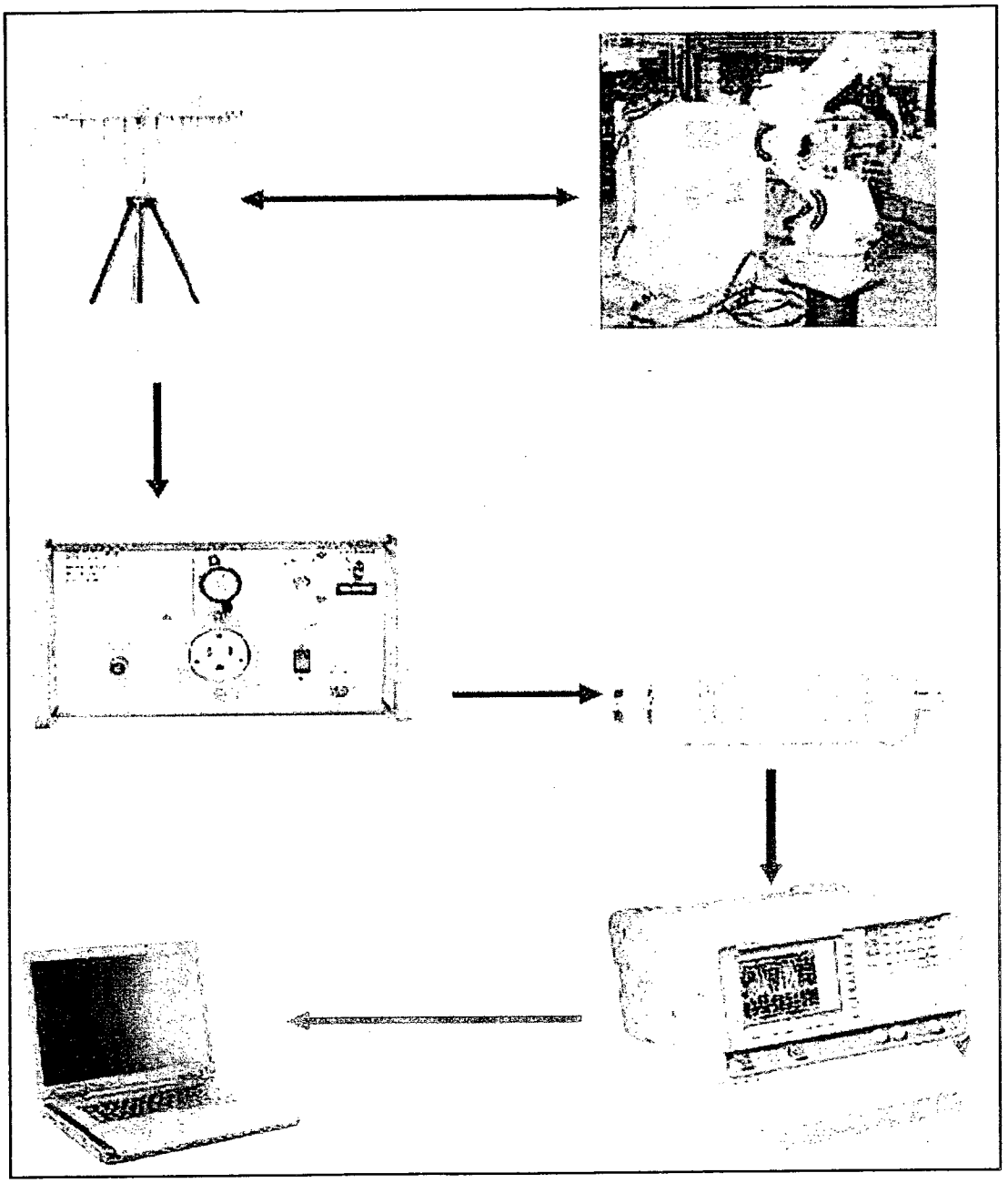

(b)

Figure 3.3 (b) EMI Measurement Equipment Setup

- The Device Under Test (DUT) represents any of the mentioned equipment around which the EMI measurements were investigated.

- The Line Impedance Stabilization Network (LISN) was used to filter the mains voltage and block higher-than-mains frequencies. Moreover, the LISN generates a characteristic impedance of 50 Ω to the DUT. The LISN is simply a RLC π-network filter.
- The Log-Periodic Antenna was used for the frequency range of *300-1900 MHz* Type N connectors were used to hook the antenna to the 3-meter cable being fed into the EM analyzer. The antenna was used in both vertical and horizontal polarizations to take the measurements.
- The Agilent EM analyzer was used to capture and monitor the peak radiated EMI levels with different frequency sweeps and to measure both the peak and RMS values in dBμV.

The absolute value of the measured radiated electric field can be formulated taking several antenna and spectrum analyzer properties as correction factors. Mathematically, the relation will be [1]:

$$\left|E_{measrured,dB\mu V/m}\right| = \left|V_{SA}\right|_{dB\mu V} + \chi_{cable,dB} + 20\log_{10} f + \left|F_{GP,dB}\right| - \left|Z_{probe,dB\Omega}\right| - 13.58 \qquad (3.10)$$

The definitions and empirical values of all the parameters in (10) are presented in Table 3.1. Moreover, the values for the ground plane coefficients (horizontal polarization) at various frequencies and antenna heights are provided in [1].

$\lvert V_{SA}\rvert_{dB\mu V}$	Measured Spectrum Analyzer Signal Voltage	38 dBμV
$\chi_{cable,dB}$	Cable Factor	1 dB
$20\log_{10}f$	The logarithmic frequency	40 dB
$\lvert F_{GP,dB}\rvert$	Ground Plane Coefficient Correction Factor	0.78 dB
$\lvert Z_{probe,dB\Omega}\rvert$	Current Probe's Transfer Impedance	15 dBΩ

Table 3.1 Correction Factors of the Total Measured Radiated EMI at 100 MHz

$\lvert V_{SA}\rvert_{dB\mu V}$	Measured Spectrum Analyzer Signal Voltage	52 dBμV
$\chi_{cable,dB}$	Cable Factor	1 dB
$20\log_{10}f$	The logarithmic frequency	60 dB
$\lvert F_{GP,dB}\rvert$	Ground Plane Coefficient Correction Factor	-14 dB
$\lvert Z_{probe,dB\Omega}\rvert$	Current Probe's Transfer Impedance	15 dBΩ

Table 3.2 Correction Factors of the Total Measured Radiated EMI at 1 GHz

3.3 EMI Measurement Results

The following Tables summarize the radiated EMI measurements conducted 10m from each of the factory floor equipment. These measurements have been tabulated from the notes and graphs obtained from the EM analyzer. The results will be further analyzed and used in the design of band reject filters of Chapter 4. Figure 3.4 illustrated the measuring equipment in the vicinity of a stationary robot gantry.

Any deviation of the radiated EMI level from the limits imposed by the FCC is highly undesirable. Efficient EMI mitigation circuits are needed to reduce the adverse effects of EMI and to achieve higher quality of wireless data communications [3].

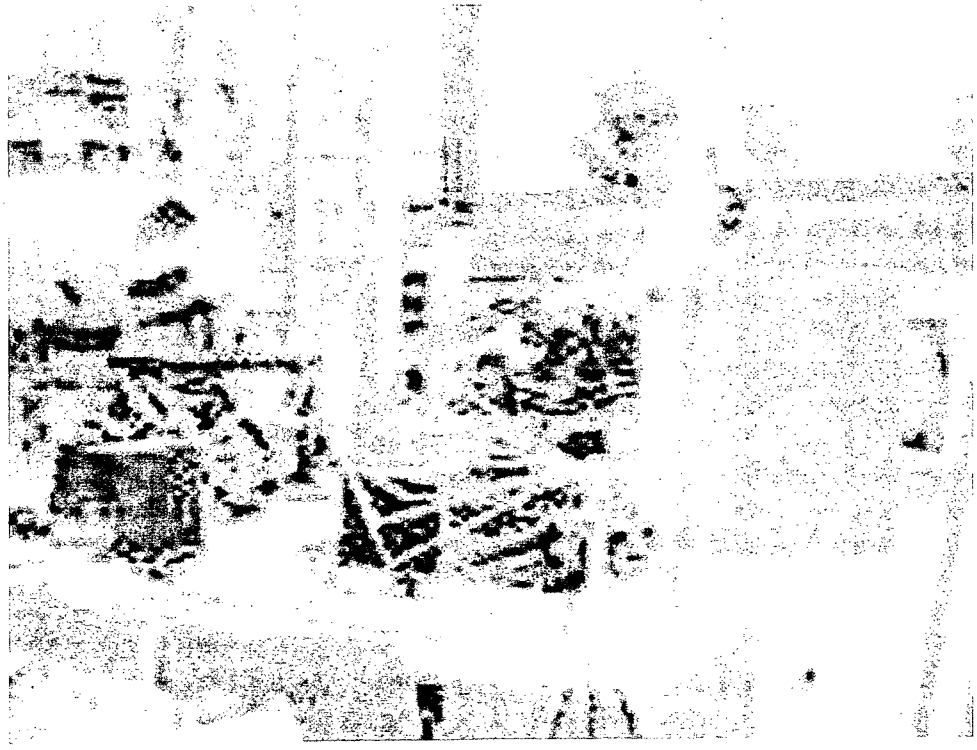

Figure 3.4 EMI Measurement Site near Robot Controller

Tables 3.3 - 3.5 outline the average measured radiated EMI in the vicinity of the robotic controller, wireless receiver, and its adverse nonlinear impacts on the quality of communication. The FCC standards on the radiated EMI are also indicated on the tables.

Peak Frequency (MHz)	**Measured Radiated EMI $S_{r,meas}$ (dBμV/m)**	**FCC Limit on Radiated EMI $S_{r,lim}$ (dBμV/m)**	**Marginal Difference $\Delta_m = S_{r,meas} - S_{r,lim}$ (dB)**
124	40.2	43.5	-3.3
220	45.2	46.4	-1.2
307	51.4	46.4	5
320	67.8	46.4	21.4
497	64.2	46.4	17.8
530	66.1	46.4	19.7
680	63.2	46.4	16.8
704	62.7	46.4	16.3
840	66.7	46.4	20.3
1080	60.4	46.4	14
1350	69	49.5	19.5
1464	77.2	49.5	27.7

Table 3.3 Measured Radiated EMI 10 m from Robotic Controller (Operation Mode)

Peak Frequency (MHz)	Measured Radiated EMI $S_{r,meas}$ (dBμV/m)	FCC Limit on Radiated EMI $S_{r,lim}$ (dBμV/m)	Marginal Difference $\Delta_m = S_{r,meas} - S_{r,lim}$ (dB)
229	47.2	46.4	0.8
293	51.3	46.4	4.9
307	52.7	46.4	6.3
384	53.4	46.4	7
432	60	46.4	13.6
574	54.8	46.4	8.4
637	61.5	46.4	15.1
701	63.8	46.4	17.4
745	50.8	46.4	4.4
860	52.3	46.4	5.9

Table 3.4 Measured Radiated EMI 10 m from the Robot (Stationary Mode)

Peak Frequency (MHz)	Measured Radiated EMI $S_{r,meas}$ (dBμV/m)	FCC Limit on Radiated EMI $S_{r,lim}$ (dBμV/m)	Marginal Difference $\Delta_m = S_{r,meas} - S_{r,lim}$ (dB)
201	49.3	46.4	2.9
245	51.5	46.4	5.1
304	60	46.4	13.6
361	63.4	46.4	17
415	62.5	46.4	16.1
572	70	46.4	23.6
603	64.6	46.4	18.2
673	60.7	46.4	14.3
734	50.1	46.4	3.7
806	51	46.4	4.6
859	63.8	46.4	17.4
908	62.7	46.4	16.3
920	62.7	46.4	16.3

Table 3.5 Radiated EMI (Measured 10 m from the Friction Stir Welding Machine)

3.4 Analysis of the Measurements

The radiated EMI limits governed by the FCC are outlined in [1] for Class A industrial electrical equipment. The measured radiated EMI levels of Tables 3.3 - 3.5 have been compared against those limits. As observed in the tables, the marginal difference, Δ_m, has been calculated as the difference between the measured level and the limit at each corresponding frequency.

According to the FCC Class A limits on the industrial equipment, the operation frequencies at which the radiated emissions were unacceptable involves those that exhibit a significant Δ_m. Due to limited resources and complexity of filter design and manufacturing, the primary focus of this research work is on the frequencies at which the values of $\Delta_{m\ are}$ greater than or equal to 15 dB. The frequencies corresponding to the measured EMI levels having marginal difference higher than 15 dB will be used as the center frequencies of the band reject filters of next chapter.

The goal of designing the band stop filters (BSFs) of next chapter is to provide stable and selective filtering of the unwanted frequencies outlines in Tables 3.3 - 3.5 in the vicinity of the main robotic controller. These filters have been designed and fabricated such that they can be mounted on the wireless receiver that is connected to the controller's Input/Output (I/O) unit via standard 50-Ω BNC connectors. Depending on the robotic motion, placement of the wireless receiver, and the ambient equipment being used, the appropriate filter can easily be connected and used while the robotic arm is controlled

wirelessly. The selected center frequencies of the designed band stop filters for the next chapter involve those corresponding to Table 3.3, due to the more frequent operation of the robotic controller independent of friction stir welding tasks.

3.5 Summary of Chapter 3

In this chapter the radiated EMI level measurements were tabulated and compared against the FCC limits on them at frequencies of 300 - 1800 MHz. The measurement equipment setup was illustrated and descriptions of the equipment have been provided. Finally, the results have been analyzed, where the frequencies of interest for the filter design correspond to those at which the marginal difference between the measured and regulated radiated EMI levels near the robotic controller were higher than 15 dB.

Chapter 4

EMI Filter Design

4.1 Background and Theory

Many applications of modern electronic communications and microwave systems require filtering only a specified spurious band of frequencies. Planar BSF technology is practically desirable due to compact physical dimensions, low fabrication cost, high selectivity, and wide stop bands.

Conventional filter design techniques such as "Butterworth" and "Chebychev" type filters are applied to design problems that require no attenuation poles, thereby being the optimal solution for high-order designs aimed at maximizing filter selectivity [30]. Elliptic filters require attenuation poles in the vicinity of their pass bands, making them the optimal solutions for high-selectivity filtering applications.

In order to properly investigate the optimal design of EMI filters aimed at suppressing unwanted frequencies at which higher-than-FCC limit radiated EMI have been measured in Chapter 3, we will start by presenting simple band reject digital filters in the major problematic frequency band of 320 - 1800 MHz.

The Insertion Loss (IL) of the electronic filter is defined as the logarithmic ratio of the power delivered to the receiver to the transmitted power [15] [31]. This crucial data is a figure of merit of a filter, which is defined as the ratio of the signal voltage level before the insertion of the filter (V_1) to that after filter insertion (V_2). Mathematically, we will have:

$$IL_{dB} = 20\log_{10}\left(\frac{V_1}{V_2}\right) \tag{4.1}$$

If the S-parameters of the filter network are being considered, the IL formula of (4.1) can be re-written as:

$$IL_{dB} = 10\log_{10}(P_{LR}), \tag{4.2}$$

where P_{LR} represents the power loss ratio. Since we are generally interested in a matched load and source, the power loss ratio, P_{LR} will become:

$$P_{LR} = \frac{1}{1-|\Gamma(w)|^2} = \frac{1}{|S_{21}|^2}, \tag{4.3}$$

where S_{21} represents the scattering parameter related to the ratio of the filter output voltage to the input voltage, given that the incident signal waves on all ports but the first one are set to zero. The square of the real part of the S_{21} can be re-written as the ratio of the power delivered to the load to that of the filter input:

$$|S_{21}|^2 = \left.\frac{P_{MatchedLoad}}{P_{InputPort}}\right|_{Z_L=Z_0} \tag{4.4}$$

Combining (4.1) - (4.4), the closed form expression for IL can be expressed as:

$$IL_{dB} = 10\log_{10}\left(\frac{1}{|S_{21}|^2}\right) \tag{4.5}$$

According to (4.5), the IL and the square of S_{21} parameter are inversely proportional. Accordingly, Table 4.1 illustrates the extreme values of IL (dB) as functions of $|S_{21}|^2$.

IL (dB)	$\|S_{21}\|^2$
0	1
10	0.1
∞	0

Table 4.1 IL as a Function of $|S_{21}|^2$

IL is the key figure-of-merit that is used in analyzing the simulation results of the BSFs of this chapter. The following section discusses the IL of the designed filters in more detail. The goal is to maximize the IL at the cutoff frequency of each filter, and to have an IL of approximately -30 dB at the cutoff frequency and -20 dB at the lower and upper frequencies of the filters.

4.2 IL and Simulation Results of the Ideal BSFs

The BSFs of this section have been designed at cutoff frequencies corresponding to the problematic frequencies explained in Chapter 3. More specifically, we will consider the measurements of Table 3.3 since most of our focus is on the operation of the robotic manipulator, being controlled by the wireless system in the presence of other equipment in the factory floor.

The plan is to first realize the lumped element model of the filters. Then, a microstrip realization of each filter will be developed and simulated using Ansoft Designer v3. Finally, the microstrip realizations of the BSFs will be fabricated by machine milling procedures. The S-parameters and the IL of the filters are of great interest to us.

Since the filters are to be used in conjunction to wireless receivers at the robotic controller end, the finished filters are to be optimally insulated and packaged to avoid any EM radiations deteriorating their performance. Moreover, in order to avoid mismatch from the BNC connectors and the series inductors of the filters, a characteristic impedance of $Z_0 = 50\ \Omega$ has been used to ensure zero reflection between the lines.

The next section deals with the actual filter models and simulation results based on the desired cutoff frequency, bandwidth, and source/load impedance of 50 Ω.

4.2.1 Ideal Filter Realizations

Figure 4.1 illustrates a typical lumped-element model using transmission lines to realize an initial model of the BSF with cutoff frequency of 320 MHz, with peak selectivity of -100 dB.

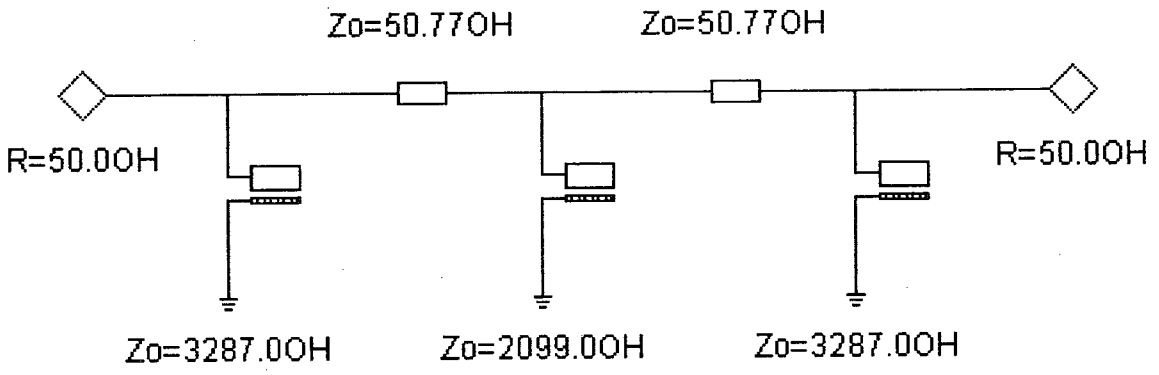

Figure 4.1 (a) Lumped Element Model

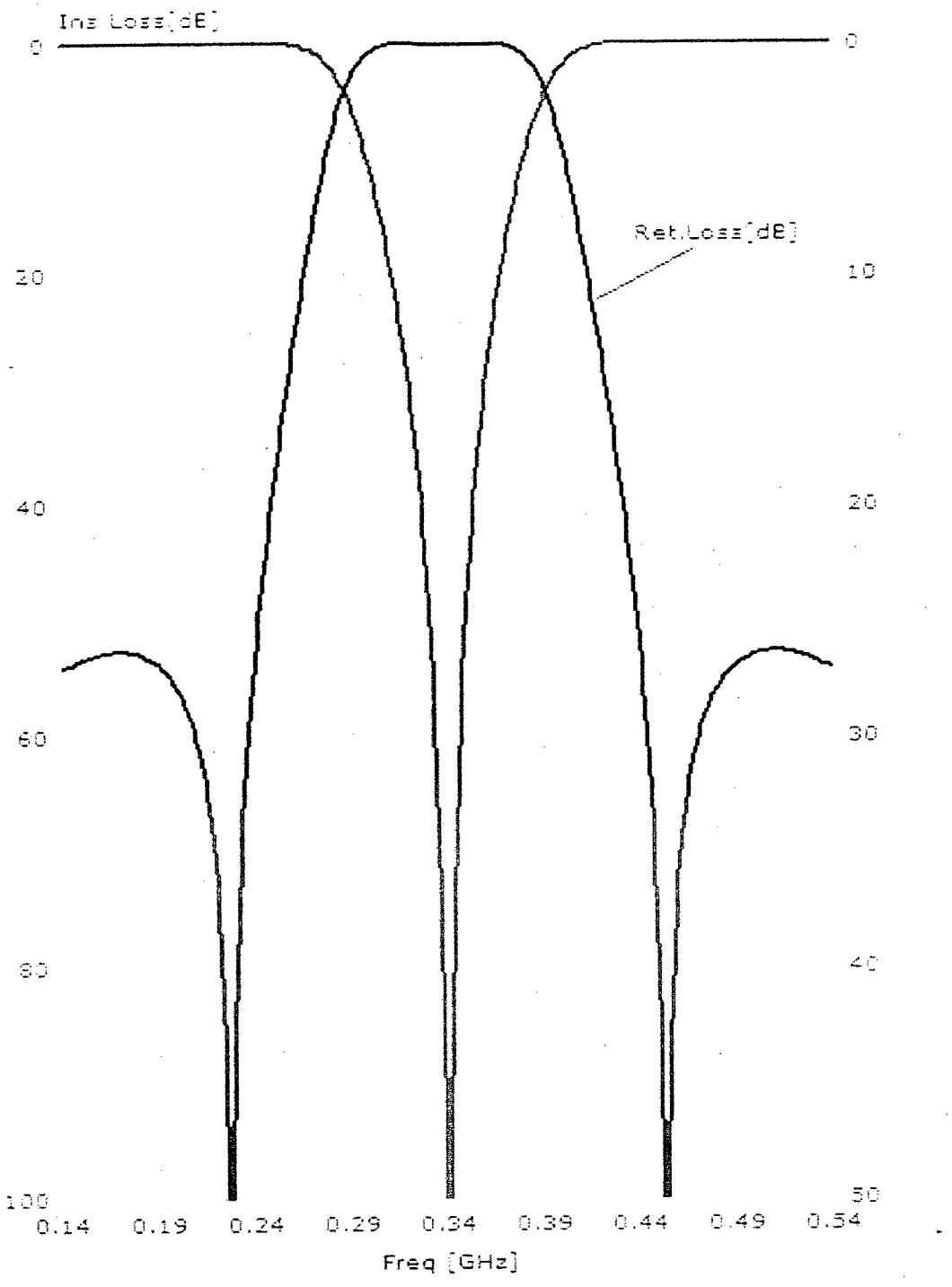

(b)

Figure 4.1 (b) Response of BSF (f_c = 320 MHz)

Other filters at higher cutoff frequencies have been developed, whose simulated responses have been illustrated in Figures 4.2 - 4.8.

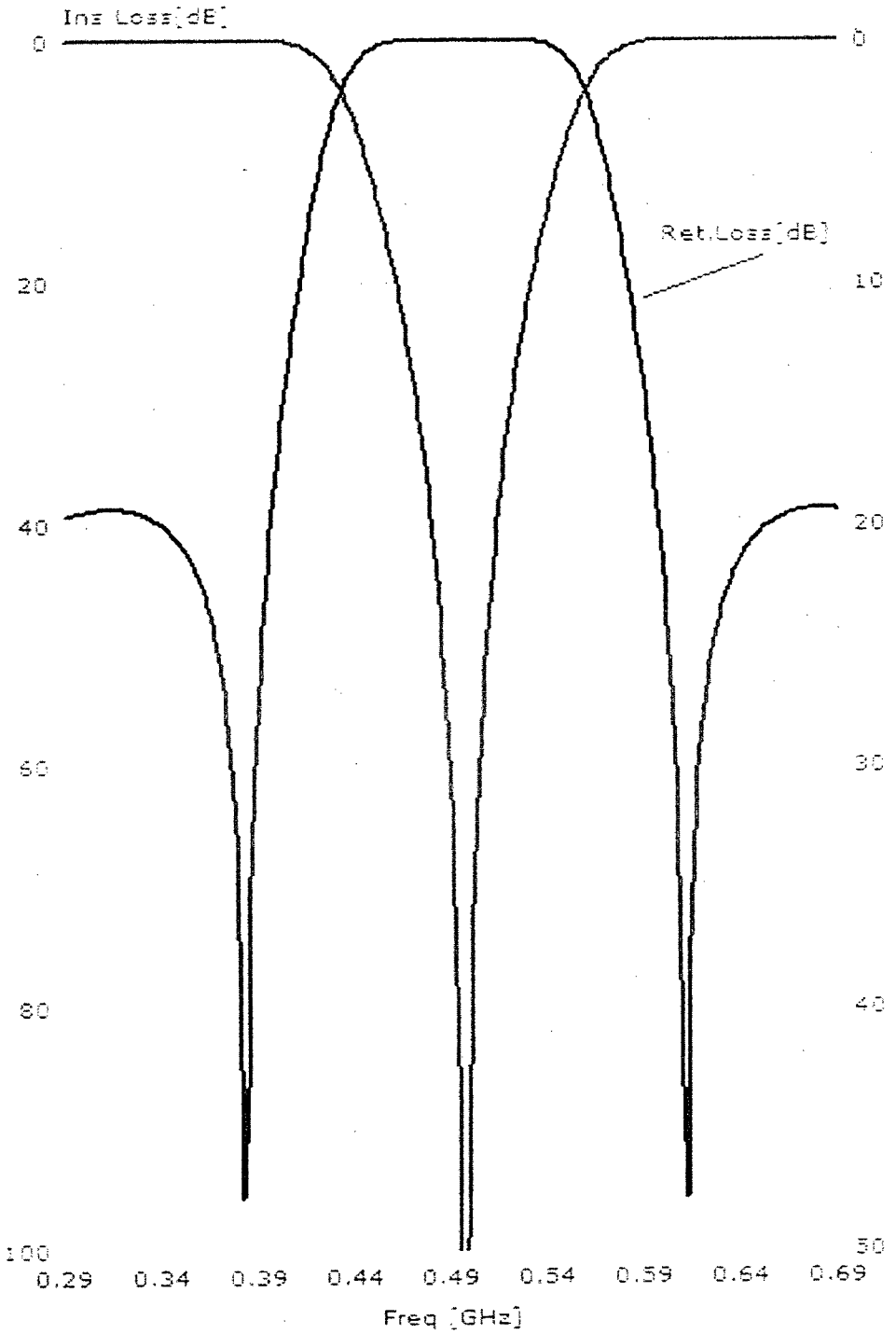

Figure 4.2 Realization of BSF (f_c = 497 MHz)

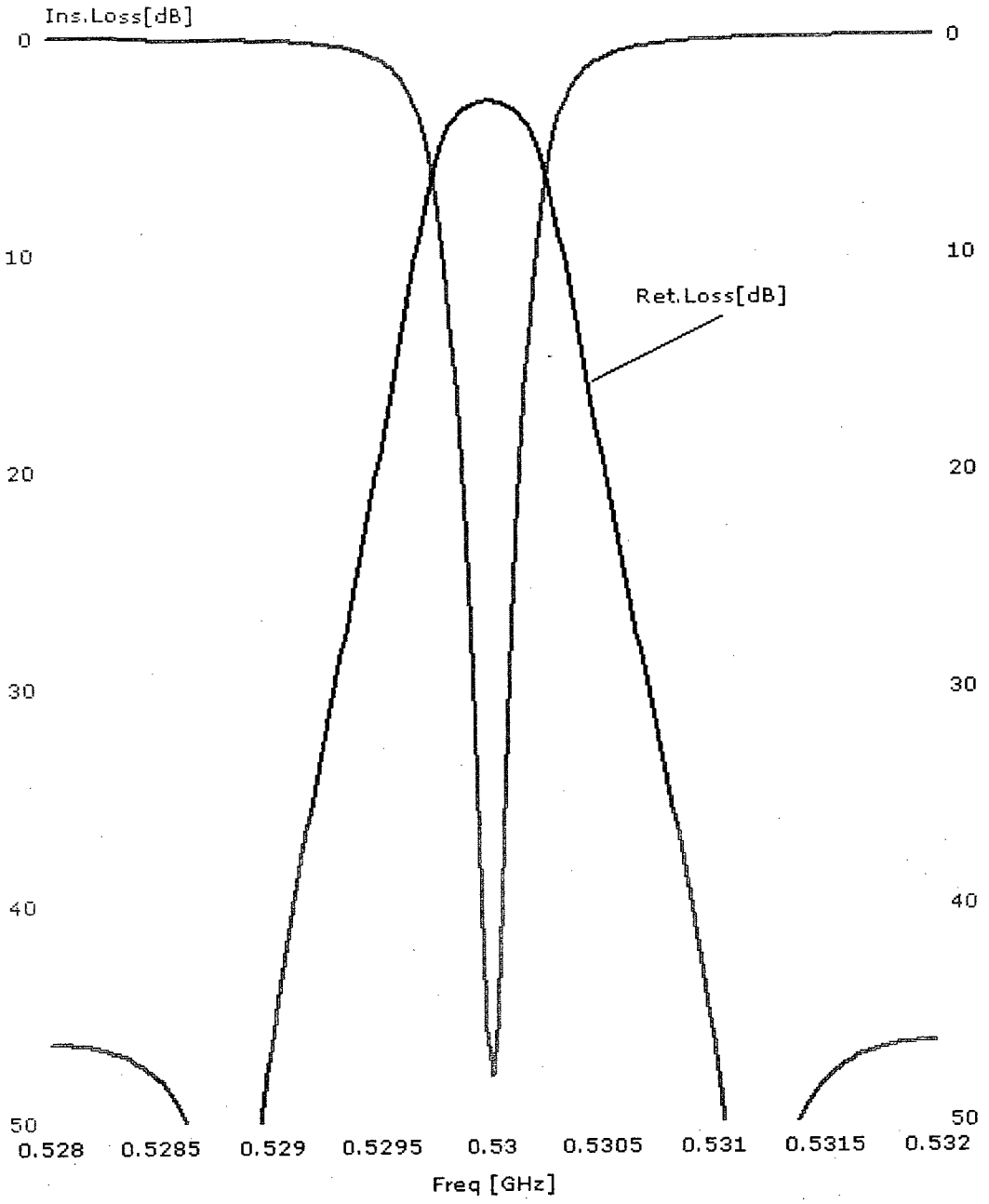

Figure 4.3 Realization of BSF (f_c = 530 MHz)

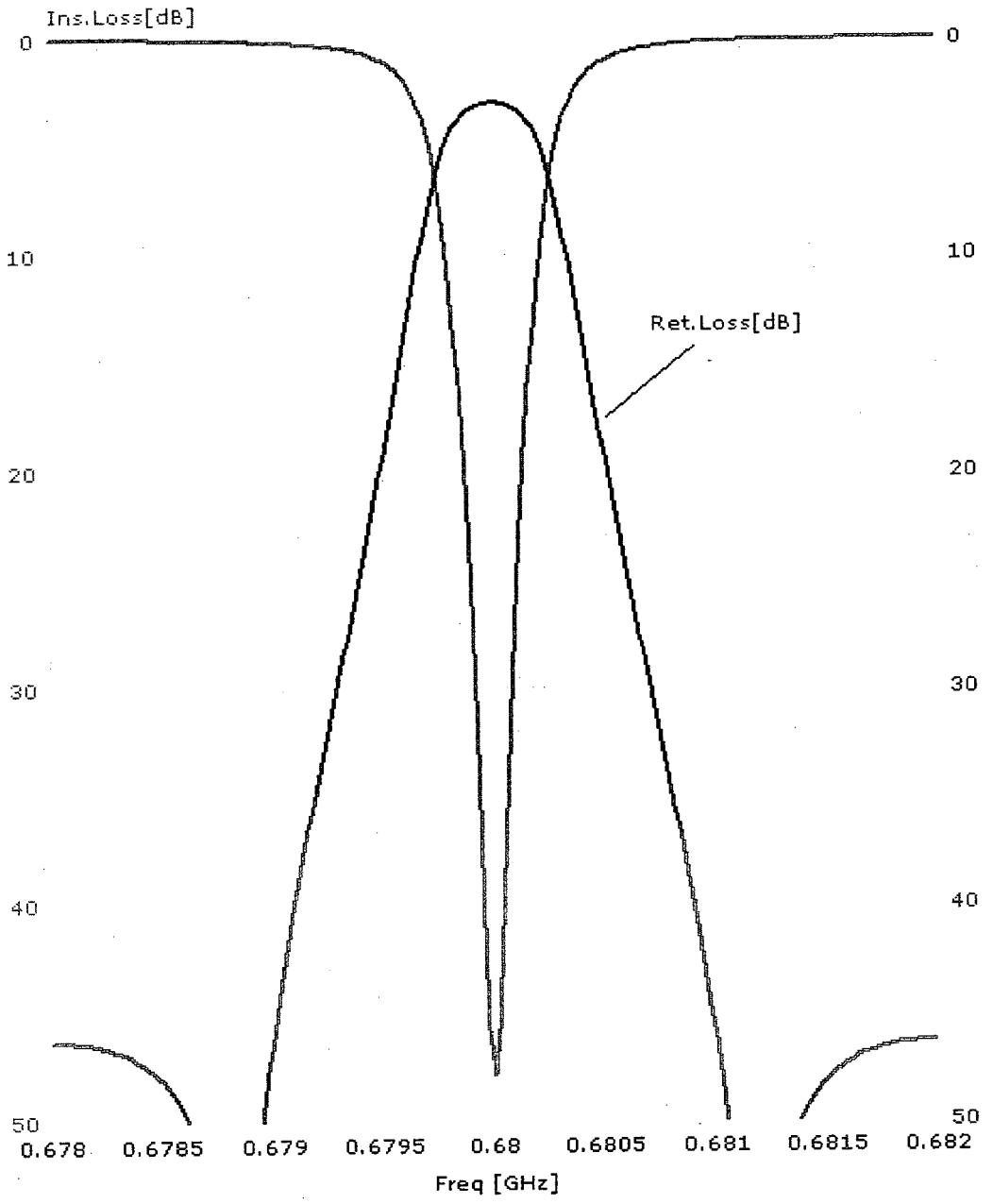

Figure 4.4 Realization of BSF (f_c = 680 MHz)

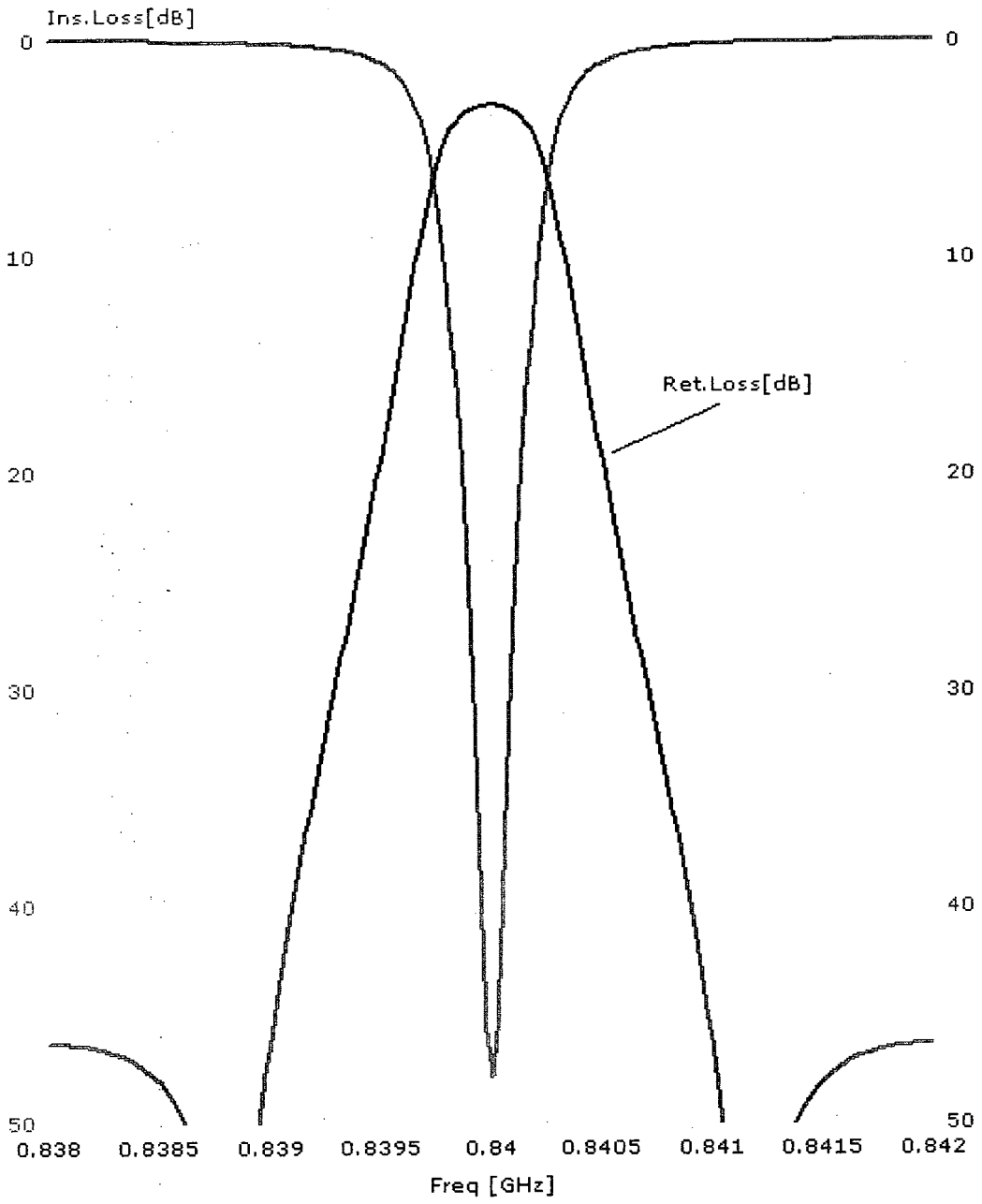

Figure 4.5 Realization of BSF (f_c = 840 MHz)

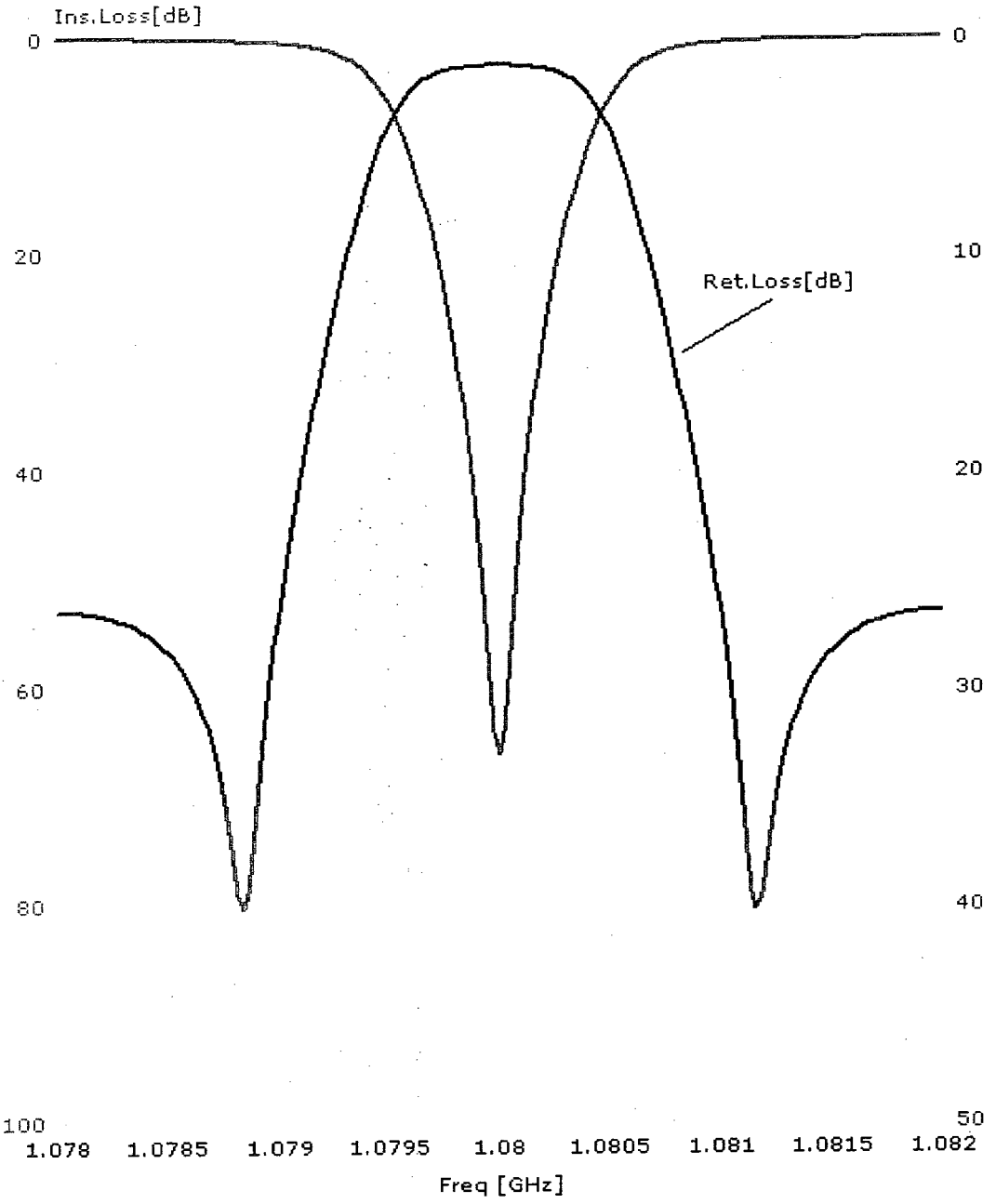

Figure 4.6 Realization of BSF (f_c =1080 MHz)

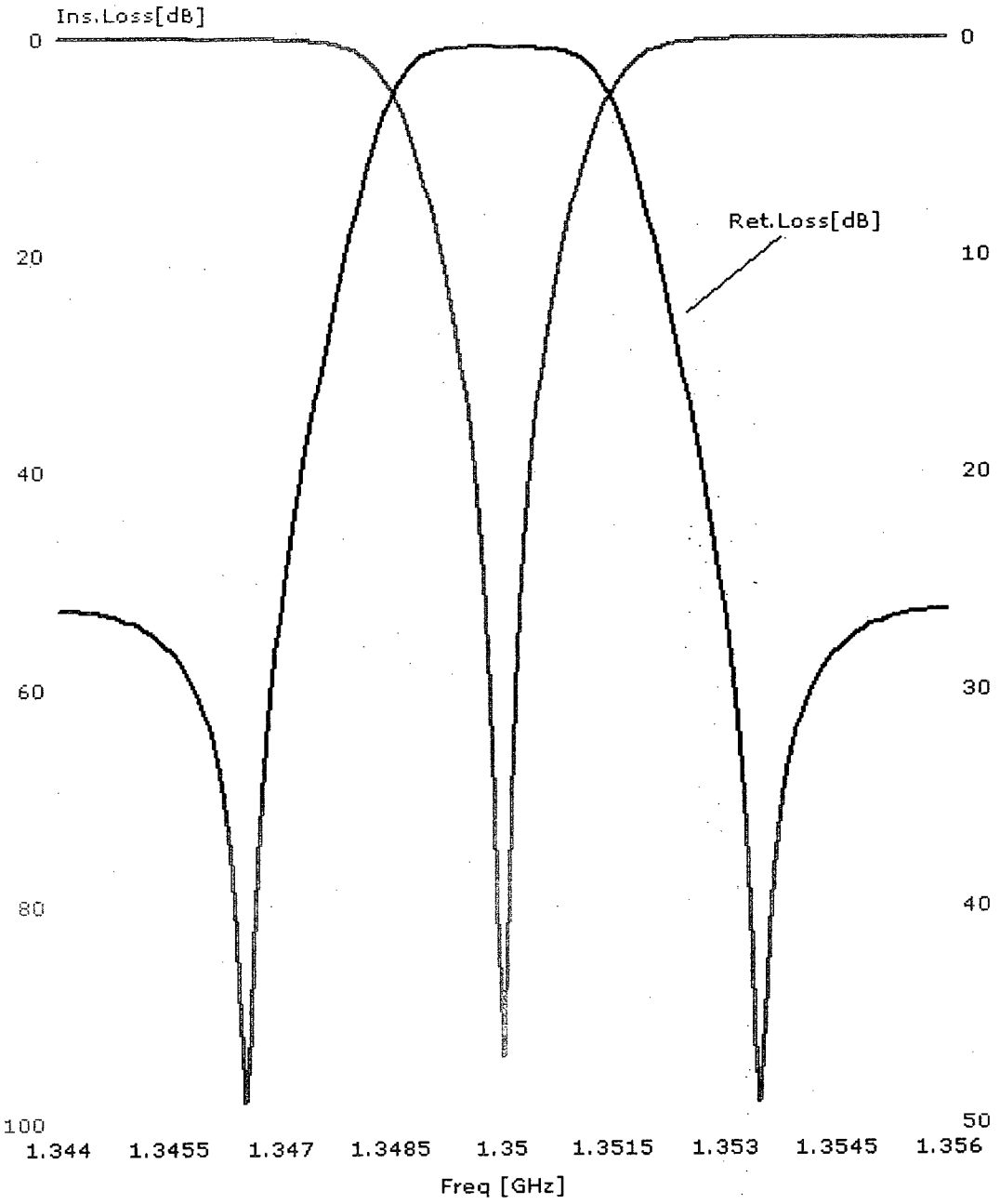

Figure 4.7 Realization of BSF (f_c = 1350 MHz)

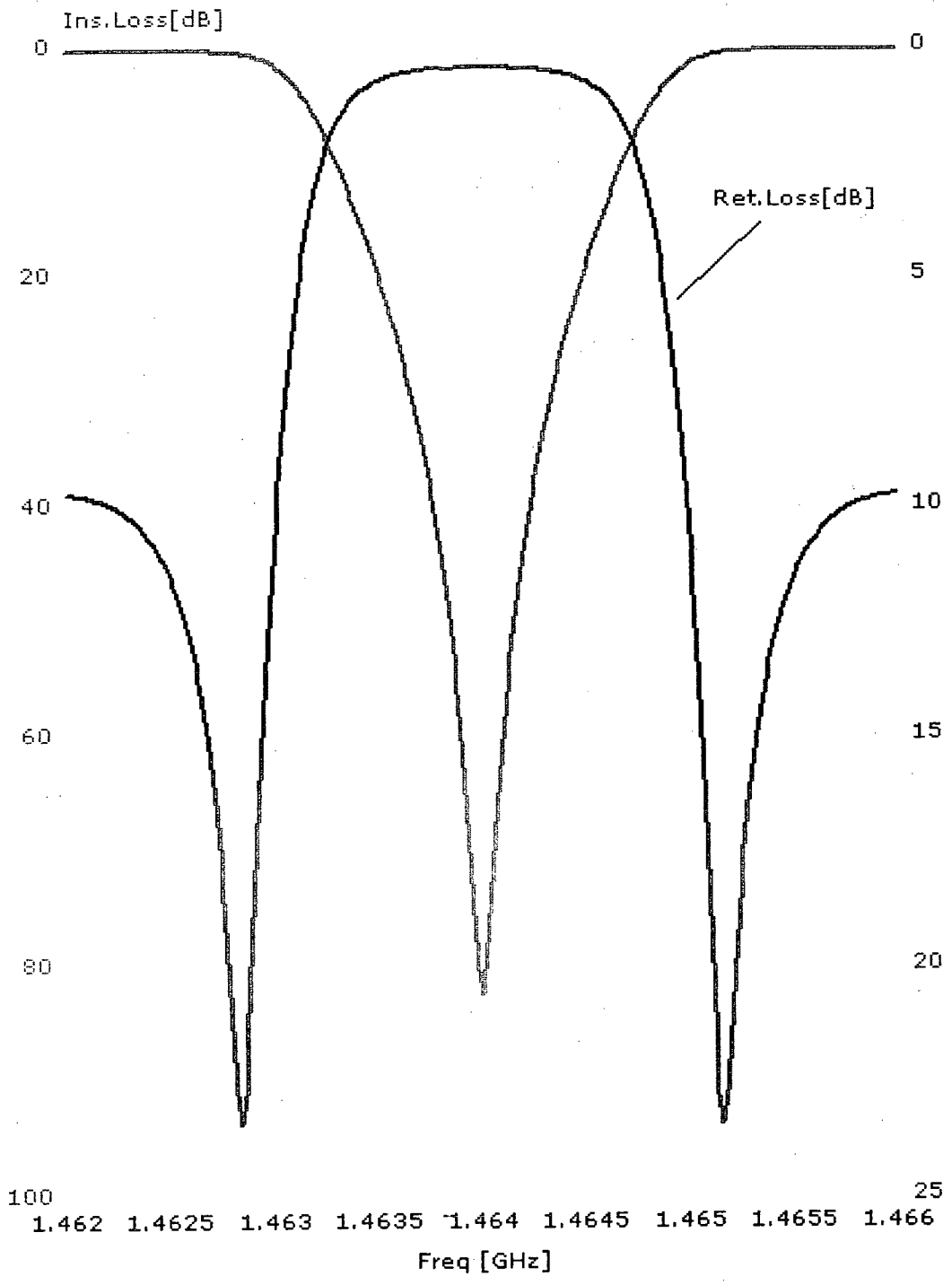

Figure 4.8 Realization of BSF (f_c = 1464 MHz)

In the next section, we will translate the mentioned filters into their microstrip line realizations. The new filters will be simulated using the same software, and the dimensions and details of the transmission lines will be explained in detail. This transformation will then enable us to fabricate the actual filters on dielectric substrates using transmission line technology.

4.3 Designed BSFs using Microstrip Technology

4.3.1 Background and Theory

Microwave components such as filters and antennas can be realized by chemical itching or milling of metal patterns on a substrate. The substrate consists of a layer of dielectric substrate sandwiched between two layers of substrates, one of which is the ground and the other one is typically air. Figure 4.9 (a) illustrates the cross section of a typical microstrip layout, consisting of top and ground metal plates, dielectric material, and the top layer on which the conductor strip gets milled. Figure 4.9 (b) is a 3D image of the actual Rogers RT/duroid® 5880 high-frequency laminate simulated in Ansoft Designer v3 for design purposes. The 3D image has been scaled to the Z-axis and shows the top layer of the board.

Figure 4.9 (a) Cross Sectional view of a Typical Microstrip

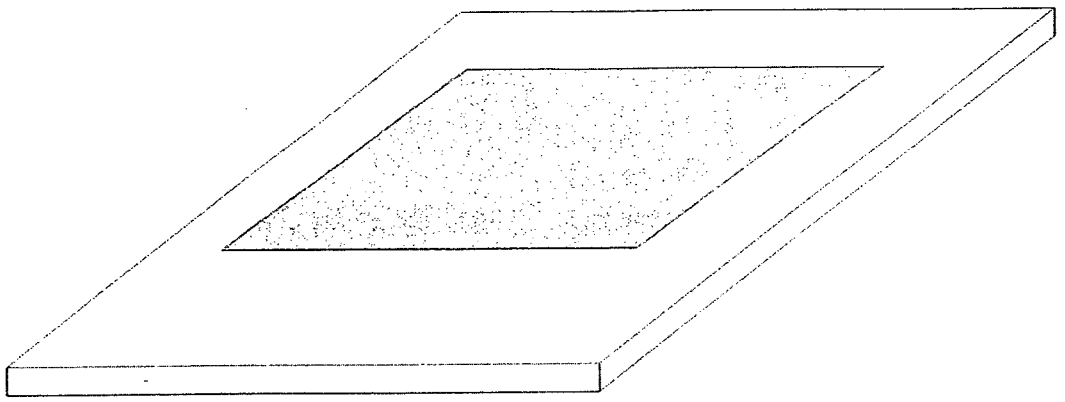

(b)

Figure 4.9 (b) 3D View of the Rogers RT/duroid® 5880 in Ansoft Designer

The above-mentioned filters can be realized by machine-milling conductor strips of a certain thickness on the Rogers RT/duroid® 5880 laminates. Microstrip circuits are typically more economical and compact than their waveguide counterparts. On the other hand, microstrip filters exhibit higher losses. The other disadvantage of microstrip technology is higher losses due to the dielectric and discontinuity of the layer gaps. Moreover, unlike waveguides, microstrip filters are not enclosed, and is therefore susceptible to cross-talk and unintentional radiation.

Since this work focuses on compact dimensions, low costs, and high selectivity, the mentioned disadvantages are not of significant importance to us. If not properly shielded, microstrip filters have the potential of becoming vulnerable to spurious EM radiation. Monolithic Microwave Integrated Circuits (MMICs) implement filters and other similar passive components being built using microstrip technology. Moreover, high-speed

digital Printed Circuit Boards (PCBs) implement microstrip transmission lines, thereby ensuring minimal distortion and minimal cross-talk of signals being routed from one part of the assembly to another.

In this research work, the "Rogers RT/duroid® 5880" high-frequency laminate has been selected as the fabrication substrate. The electrical characteristics of this substrate have been summarized in Table 4.2.

Electrical Property	**Value**
Dielectric Constant, ε_r	2.2
Skin Depth, δ	0.0229 (+Z direction)
Volume Resistance	2×10^7 MΩ.cm
Surface Resistance	3×10^8 MΩ

Table 4.2 Some Electrical Properties of the Rogers RT/duroid® 5880 Laminate

These filters have been designed for center frequencies at which quasi-peak measured levels of radiated EMI have been more than the corresponding FCC limits. The microstrip models of the BSFs have been realized using transmission lines on Rogers RT/duroid® 5880. The detailed datasheet outlining substrate properties is provided in Appendix A for further information.

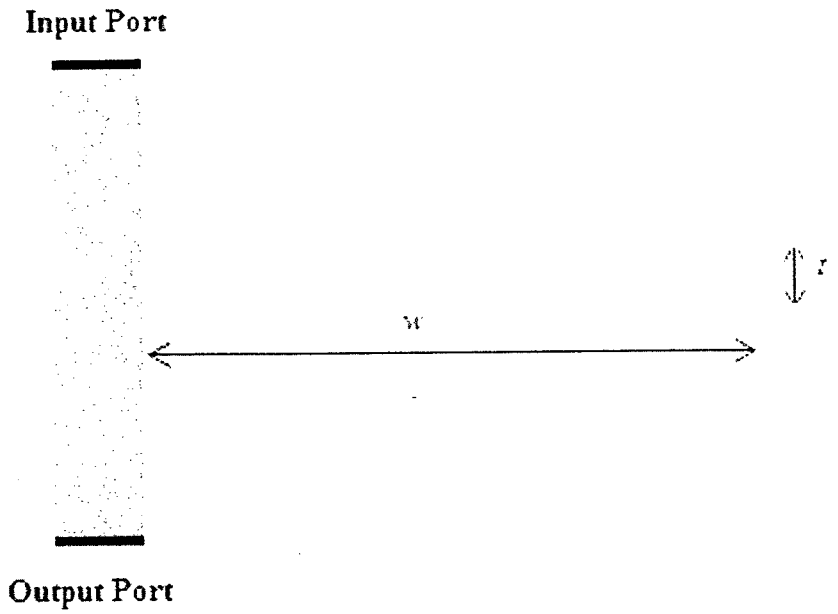

(a)

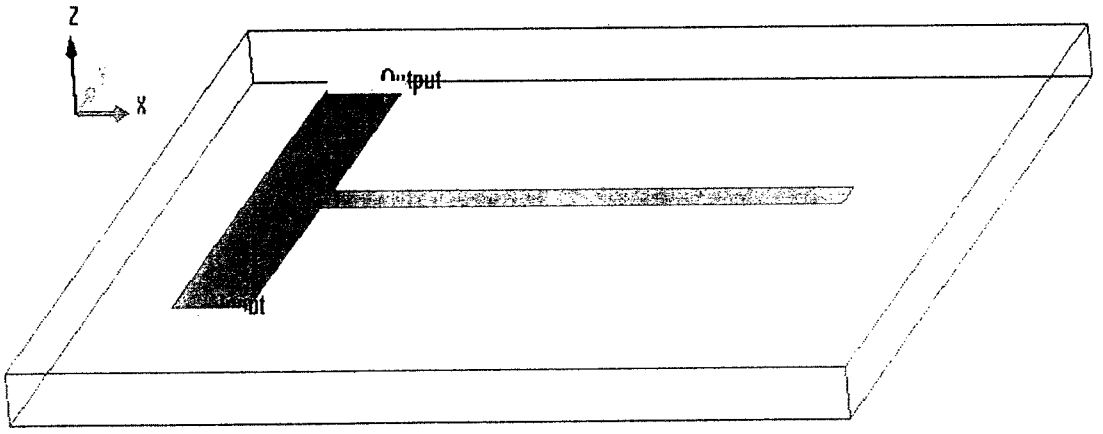

(b)

Figure 4.10 (a) Conceptual BSF for Cutoff Frequencies below 800MHz

(b) 3D Image of the Designed BSF using Ansoft Designer

As thoroughly explained in [26], the effective permittivity, ε_{eff}, for $\frac{w}{t} > 1$ can be expressed as a non-linear function of w and t (line width and thickness, respectively):

$$\varepsilon_{eff} = \left(\frac{\varepsilon_r + 1}{2}\right) + \left(\frac{\varepsilon_r - 1}{2}\right)\left[\frac{1}{\sqrt{\left(\frac{w+12t}{w}\right)}}\right] \tag{4.6}$$

Since $w >> t$ in the filter design tasks of this research work, equation (4.6) is solely used for calculating the ε_{eff} based on ε_r, w, and t.

Similarly, the characteristic impedance of the transmission line, *Zo*, can be written as [26] [31]:

$$Z_0 = \frac{\frac{120\pi}{\sqrt{\varepsilon_{eff}}}}{\frac{w}{t} + 1.393 + 0.667\ln(1.444 + \frac{w}{t})}\ \Omega \tag{4.7}$$

The effective width for a microstrip line with $\frac{w}{t} > \frac{1}{2\pi}$ is defined as:

$$w_{eff} = w + \left(\frac{1.25t'}{\pi}\right)\left[+\ln\left(\frac{4\pi w}{t'}\right)\right] \tag{4.8}$$

, where t' is the thickness of dielectric substrate and is given in the Rogers RT/duroid® 5880 laminate as 0.062 inches (≈ 1.5748 mm). Moreover, the effective permittivity, ε_{eff}, of the microstrip as a function of the line thickness, *s*, is given as:

$$\varepsilon_{eff}(s) = \varepsilon_{eff} - \left[\left(\frac{\varepsilon_r - 1}{4.6}\right)\left(\frac{\frac{s}{t}}{\sqrt{\frac{w}{t}}}\right)\right] \tag{4.9}$$

The design procedures for the microstrip BSFs involves the coupling relations between the center frequencies and the required bandwidths with the dimensions of transmission lines used for the capacitance and inductance, as well as their spacing. Since the values of ε_r and t' are given as 2.2 and 1.5748 mm, formulas (4.6) – (4.8) have been used to couple the required to calculated the line impedances corresponding to the required cutoff frequencies.

At the given substrate thickness, a line-width of 1.5 mm is being calculated to represent a line impedance of 50 Ω. Moreover, fine tuning is necessary to make sure minimal ripples are present in the IL response. In order to do this, the capacitance and inductance lines have been perfectly attached with minimal overlapped area.

The lengths of the transmission lines are calculated using equations (4.7) and (4.8), where the thickness and the characteristic impedance of the line are to be used as known variables. Finally, the transmission lines representing the shunt inductances are separated by exactly $\frac{\lambda_c}{4}$ m.

4.3.2 The Q-factor

The Q-factor determines the competence of the filter, and is defined as the ratio of the resonant frequency to the 3dB-bandwidth, which is the frequency bandwidth between the lower and upper frequencies of the filter.

In general, the loaded Q_L can be formulated as [32]:

$$Q_L = \frac{f_{resonant}}{BW_{3dB}} = \frac{f_{resonant}}{f_u - f_l} \tag{4.10}$$

In this research work, we will focus only on the loaded Q, Q_L, since it is a measurement of the coupling between the resonant circuit and the power loss at the resonant circuit at the resonant frequency [31] [32]. More specifically, the Q_L is the product of the resonant frequency and the ratio of the stored energy in the resonant circuit to the total power loss at the resonant frequency. The Q_L factors of the designed filters in the next section are calculated based on their upper and lower frequency responses, as well as their center frequencies.

4.3.3 Simulation Results

In the following designs, the dimensions of the left-most transmission line acting on behalf of the series inductor, *Ls*, is fixated at 30x5 mm. By changing the length of the

right transmission line acting on behalf of the shunt capacitor, *Cp*, we will vary the exact cutoff frequency and the attenuation of the BSF.

Figures 4.11 - 4.14 illustrate the IL responses of numerous BSFs designed by varying the length of the transmission line corresponding to the filter capacitor. The simulations have been conducted using Ansoft Designer, where both S_{11} and S_{21} parameters have been swept across appropriate ranges of frequencies. The "dB(S(Port1,Port1))" trace corresponds to S_{11}, and "dB(S(Port2,Port1))" trace corresponds to S_{21}.

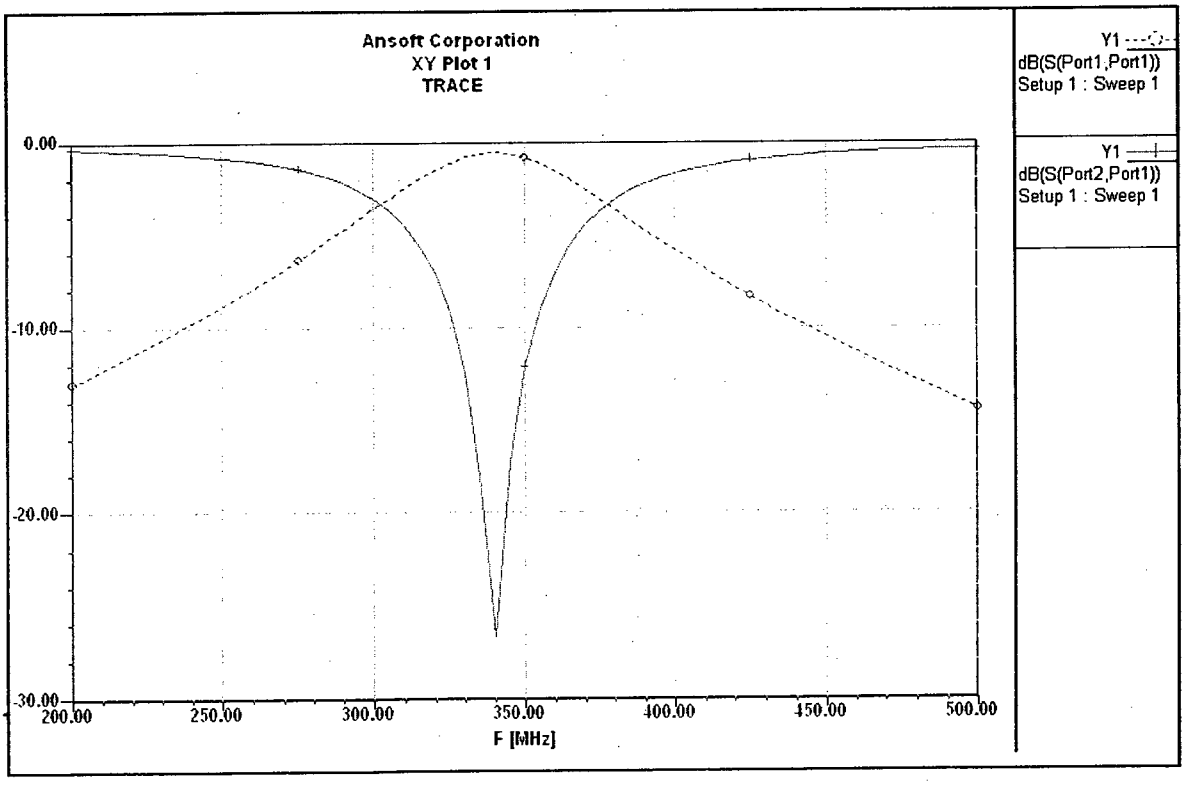

Figure 4.11 Band Reject Simulation (f_c = 320 MHz)

Table 4.3 summarizes the dimensions of transmission lines for the filters of Figures 4.11-4.14, as well as their cutoff frequencies, Q_L factors, and peak IL values.

f_c (MHz)	Shunt Capacitor Arm WxL (mm)	Series Inductor Arm WxL (mm)	Q_L	Peak Selectivity (dB)
320	158.85 x 1.5	30 x 5	5.07	-27
497	99.23 x 1.5	30 x 5	3.2	-30
530	91.66 x 1.5	30 x 5	3.19	-28.2
680	70 x 1.5 mm	30 x 5	4.01	-29

Table 4.3 Summary of the BSFs of Figures 4.11 - 4.14

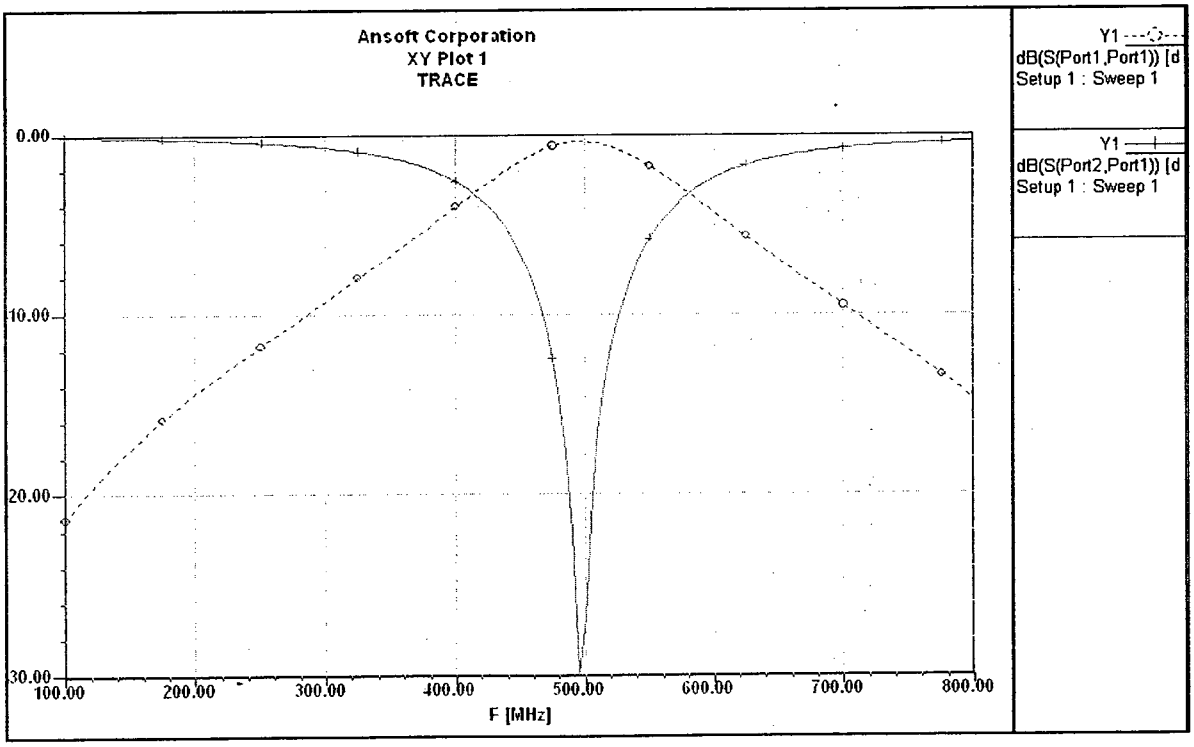

Figure 4.12 Band Reject Simulation (f_c = 497 MHz)

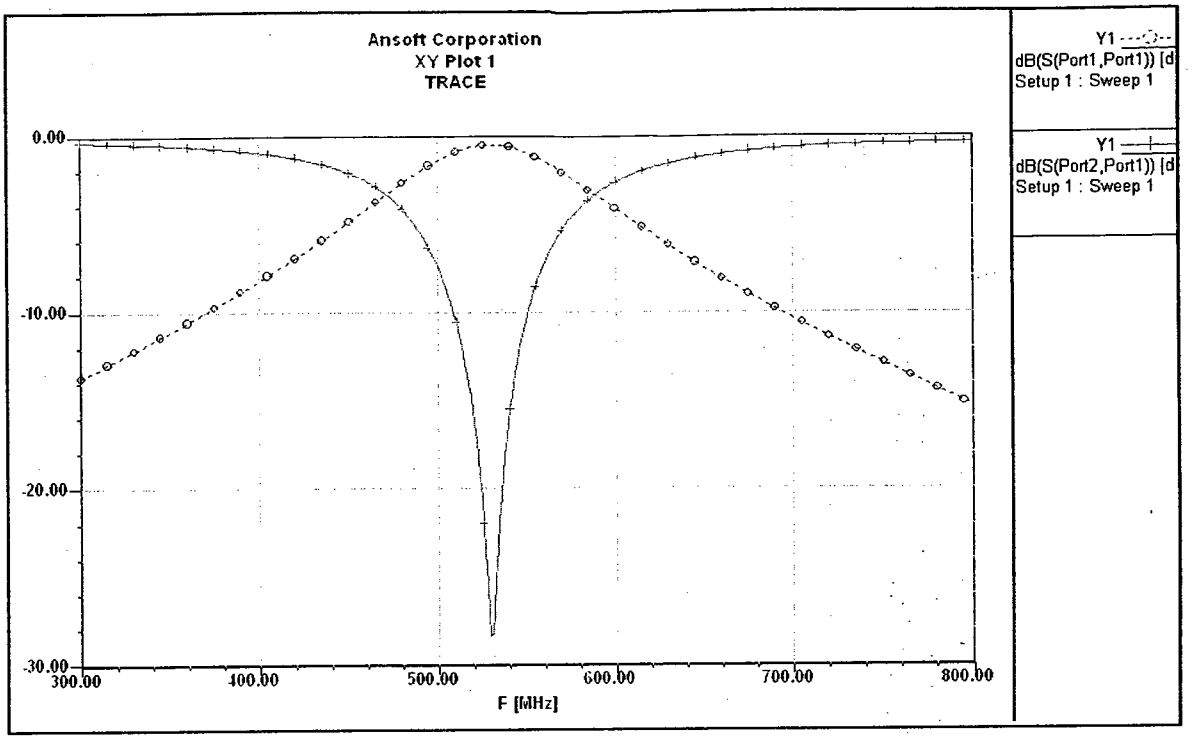

Figure 4.13 Band Reject Simulation (f_c = 530MHz)

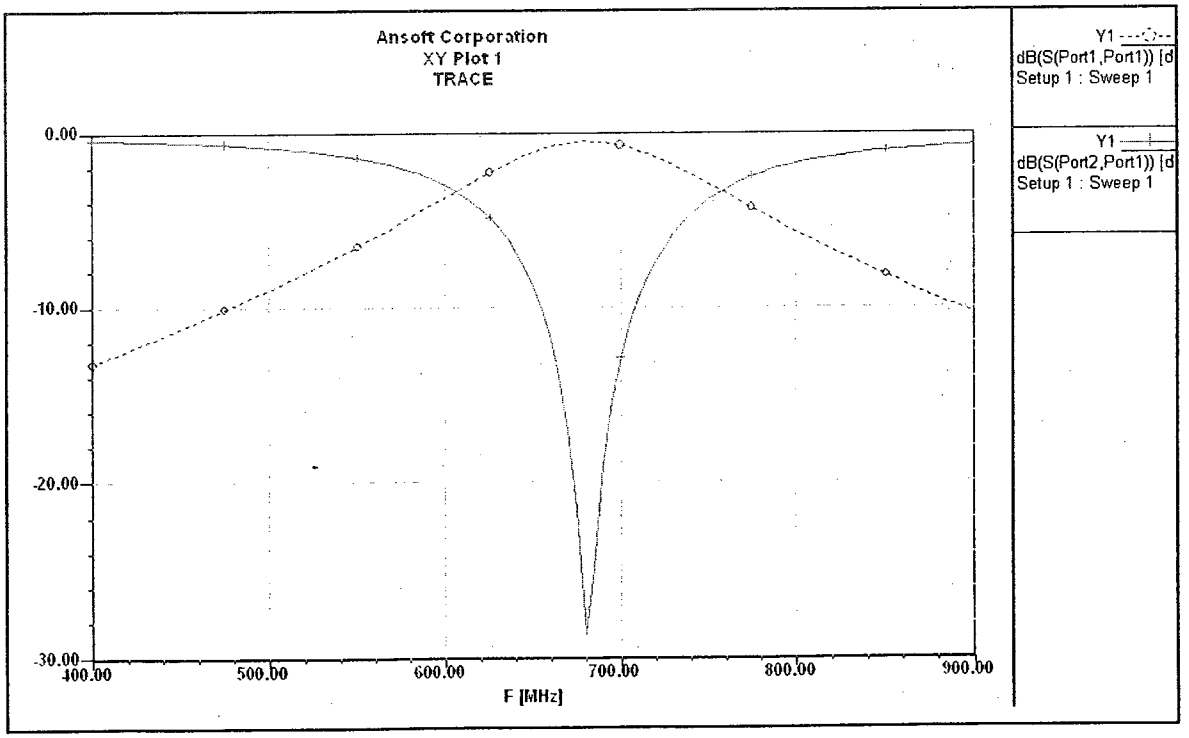

Figure 4.14 Band Reject Simulation (f_c = 680 MHz)

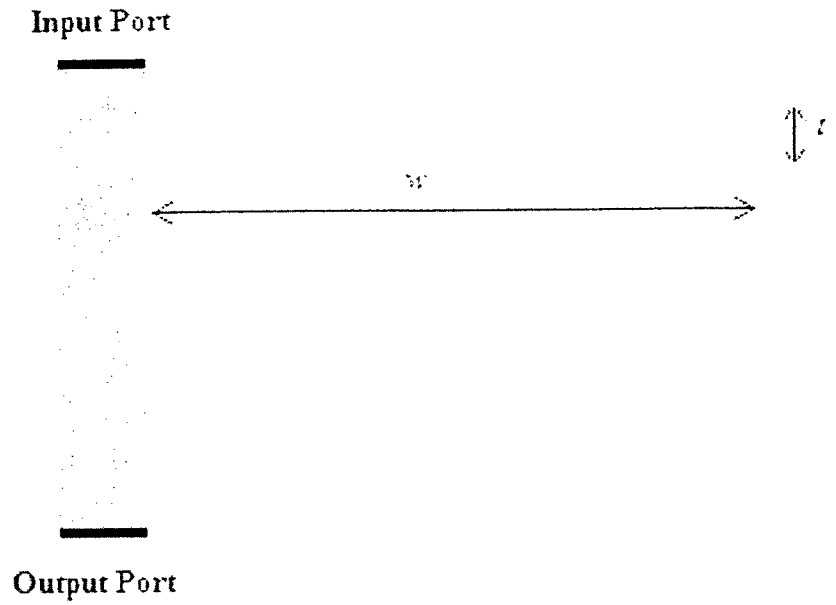

(a)

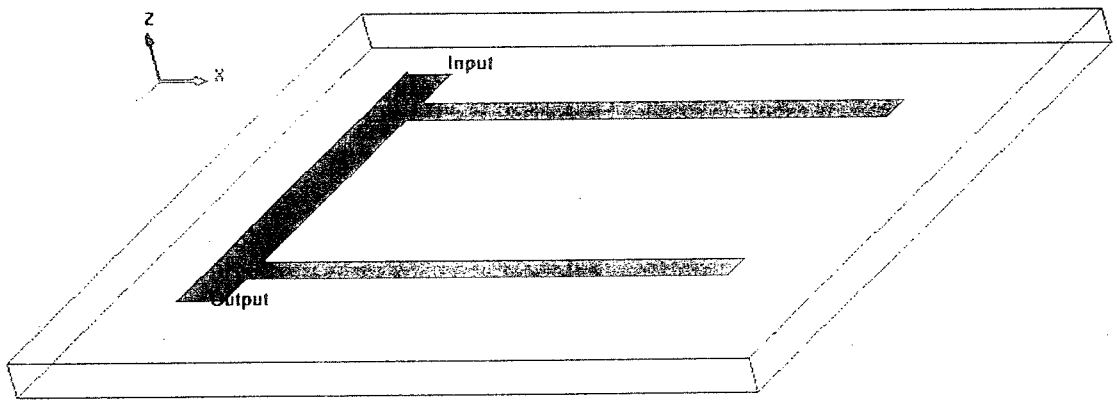

(b)

Figure 4.15 (a) Conceptual and (b) 3D Image BSF Prototype Design for Cutoff Frequencies of 840 MHz and beyond

The filter configuration illustrated in Figure 4.15 is used for BSFs having cutoff frequencies of 840 MHz and beyond. The height of the series inductor stub is adjusted

according to the frequency of interest, such that the exact separation between the two shunt capacitor stubs at each frequency is $\frac{\lambda_c}{4}$m.

We have used dual transmission lines on either edges of the stub to represent the shunt capacitor. It is important to remember that the heights of the two stubs are equal and have been reduced for these set of designs.

f_c (MHz)	Shunt Capacitor Arms WxL (mm)	Series Inductor Arm WxL (mm)	Q_L	Peak Selectivity (dB)
850	63.1 x 1.5	90 x 5	2.37	-67
1080	47.5 x 1.5	75 x 5	2.51	-42
1350	38 x 1.5	60 x 5	3.1	-75
1464	34.3 x 1.5	55 x 5	3.65	-45
1930	26.99 x 1.5	45 x 5	3.6	-69.5

Table 4.4 Summary of the BSFs of Figures 4.16 - 4.20

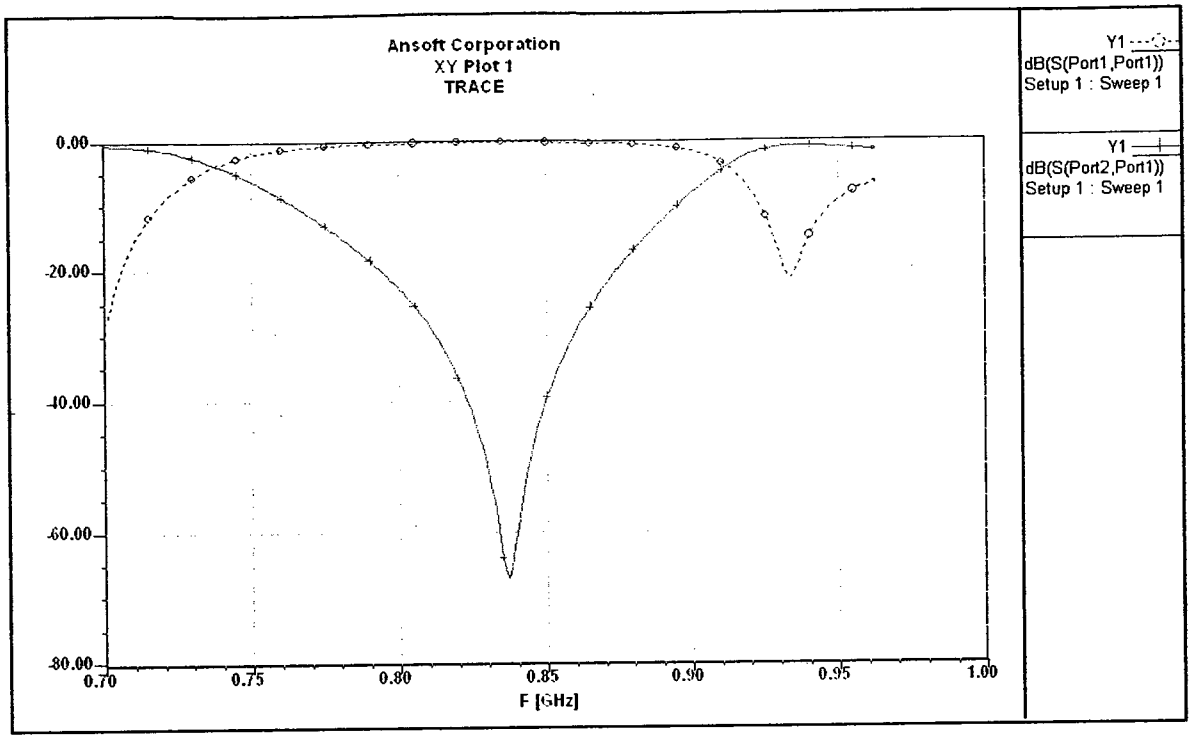

Figure 4.16 Band Reject Simulation (f_c = 840 MHz)

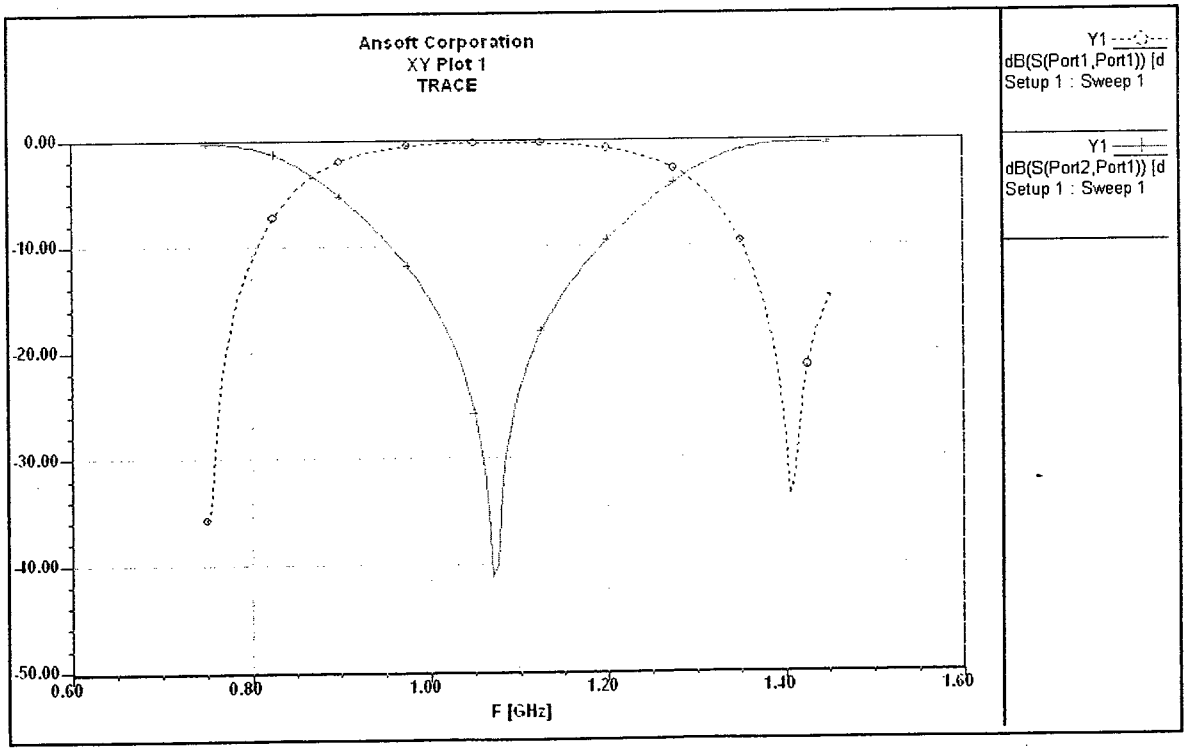

Figure 4.17 Band Reject Simulation (f_c = 1080 MHz)

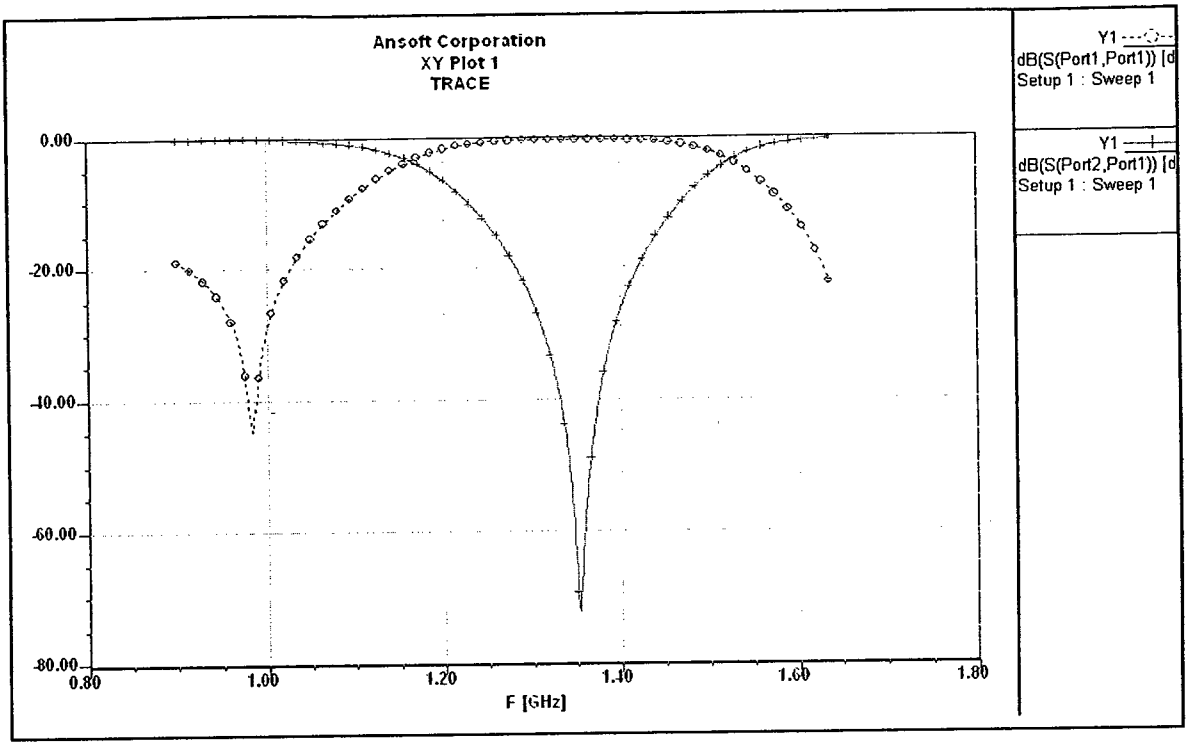

Figure 4.18 Band Reject Simulation (f_c = 1350 MHz)

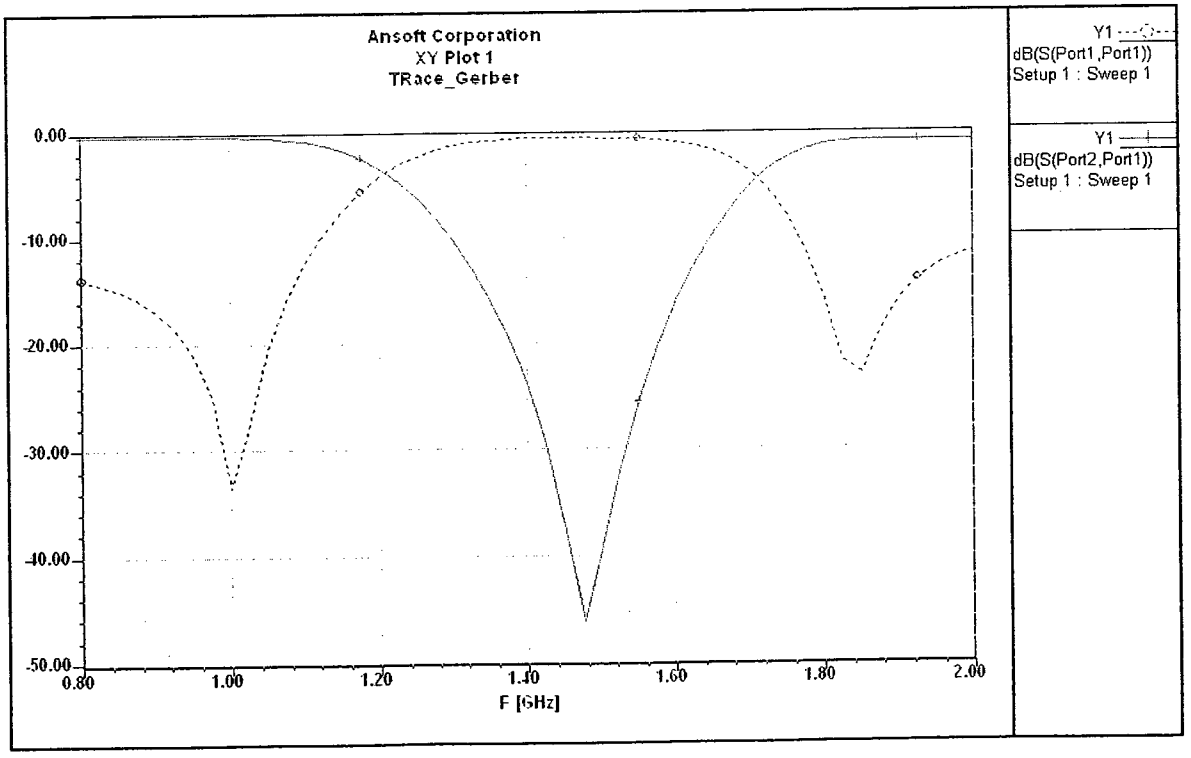

Figure 4.19 Band Reject Simulation (f_c = 1464 MHz)

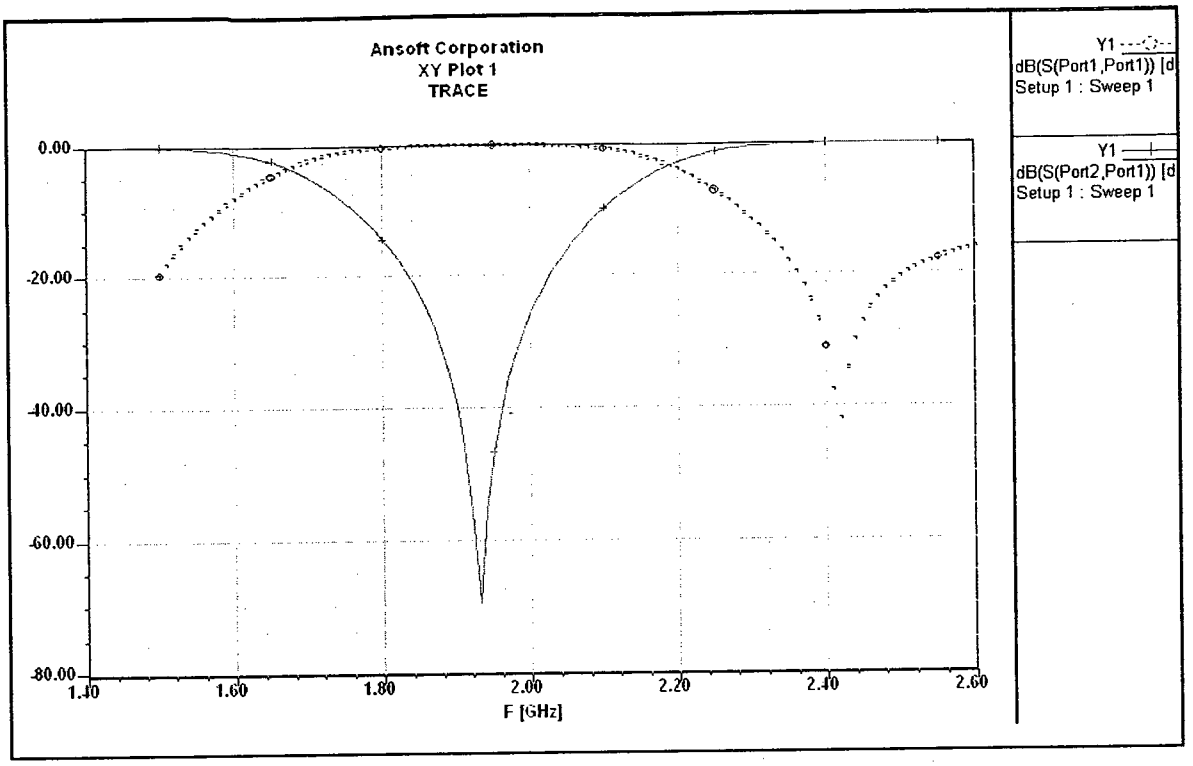

Figure 4.20 Band Reject Simulation (f_c = 1930 MHz)

4.4 Analysis of the Results

Simulation results of sections 4.2 - 4.3 demonstrate high selectivity at the specified cutoff frequencies, reasonable Q-factors, and narrow stop bands. The filters designed in this chapter will be used to suppress unwanted radiated EMI in a factory floor environment. In order to properly fabricate the designed filters on a 62-mil thick Rogers RT/duroid® high-frequency laminate, the prescribed dimensions of the transmission lines must be exactly as described in Tables 4.2 and 4.3. Moreover, in order to maximize the filter selectivity at the cutoff frequency, no discontinuity must exist between the transmission lines of the filters.

4.5 Summary of Chapter 4 & Next Research Steps

Both lumped element and microstrip models of BSFs used for EMI suppression have been designed and simulated. Chebychev and elliptical band pass filter designs have been improved in terms of gain, phase response, and the group delays. The optimum band pass filter will be Elliptic-based due to its smooth gain, phase response, and group delay. The most optimum BSF design will use the Chebychev method due to smooth phase response and similar group delay and gain [33], [34].

The next step will involve reducing the peak group delay value at higher frequency edges. Finally, a comprehensive summary on the gain, group delay, IL, and the S-parameters of the filters using transmission lines will be provided in the next two chapters.

The selectivity of the BSF plays a crucial role in determining which exact signal components are passed through and which ones are filtered [13]. The Q-factor of an RF BSF should be determined in such a way that the Adjacent Channel Selectivity Ratio (ACSR) is kept below a threshold. In the next chapter, we will define the Q-factor along with other design parameters and will use RLC network components to physically simulate both the Chebychev and Elliptic filters. To have a practically reasonable high-Q filter, we will study the positive feedback design and will also study Q-multipliers that will boost the Q factor of the filters.

Chapter 5

Filter Fabrication and Testing

5.1 Filter Prototype Fabrication

The BSFs of Chapter 4 have been built on Rogers RT/duroid® 5880 high-frequency laminates. A milling machine has been used to realize the filters on the laminates. The built BSFs are illustrated in Figures 5.1 – 5.6.

Two SM connectors have been soldered to the input and output ports of each filter in order to connect it to the Network Analyzer's ports 1 and 2. The mentioned BSFs of this section were measured for their S-parameters and their phase responses at S_{11} and S_{22} using the Hewlett-Packard (HP) 8720A Network Analyzer illustrated in Figure 5.7. The measurements have been conducted using a total of 801 equally-spaced data points in the 600-2000 MHz frequency range.

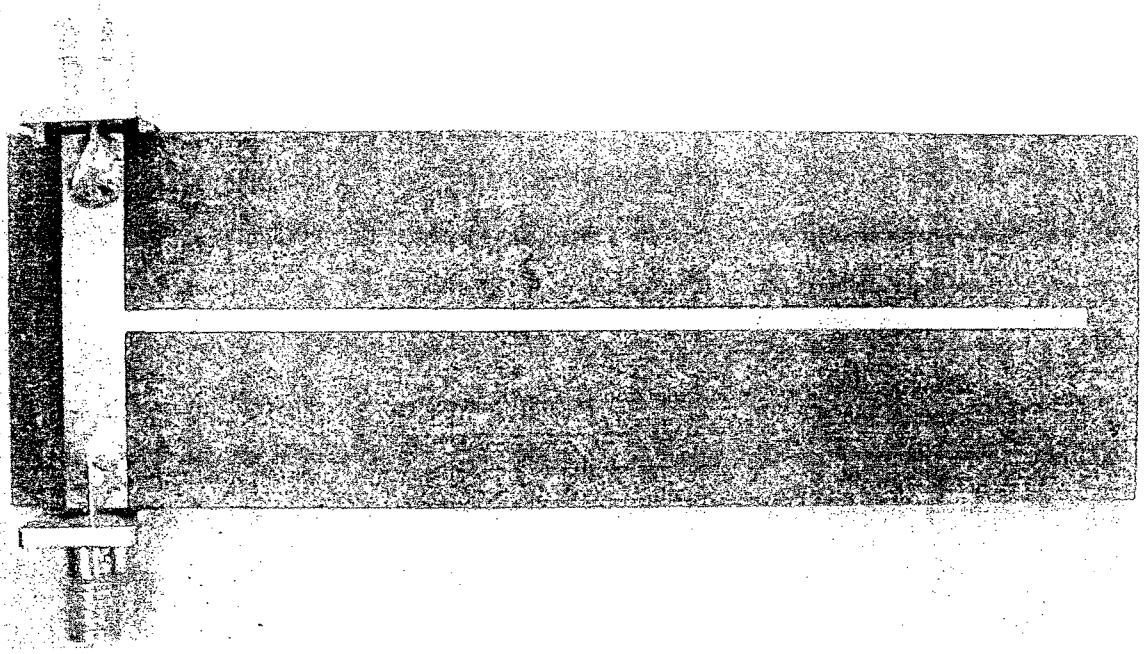

Figure 5.1 BSF Prototype (f_c = 680 MHz)

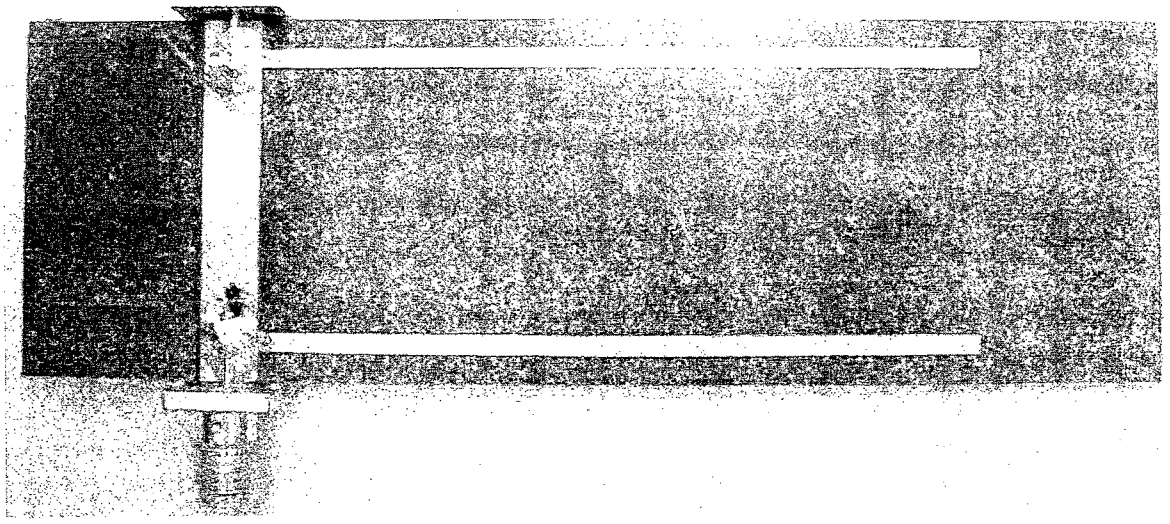

Figure 5.2 BSF Prototype (f_c = 840 MHz)

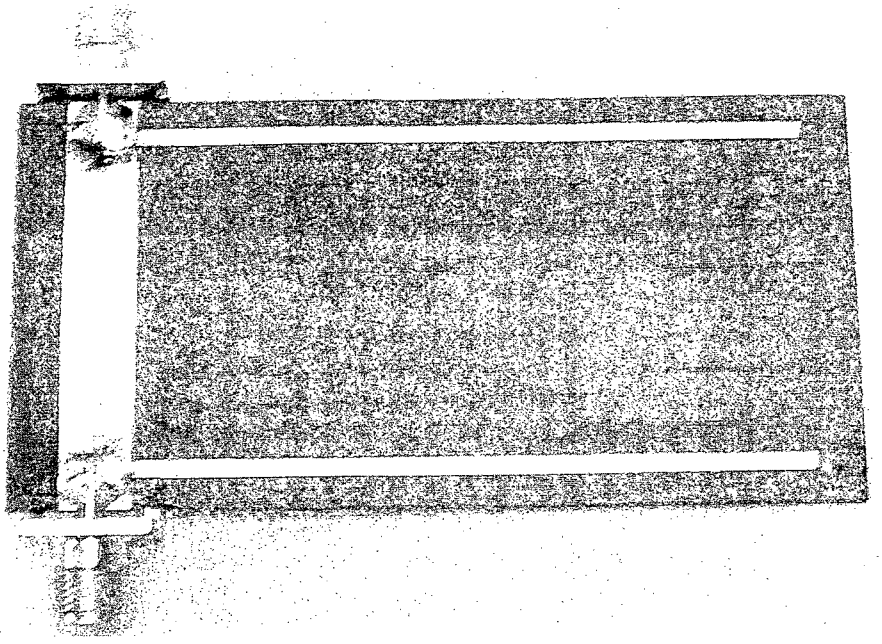

Figure 5.3 BSF Prototype (f_c = 1080 MHz)

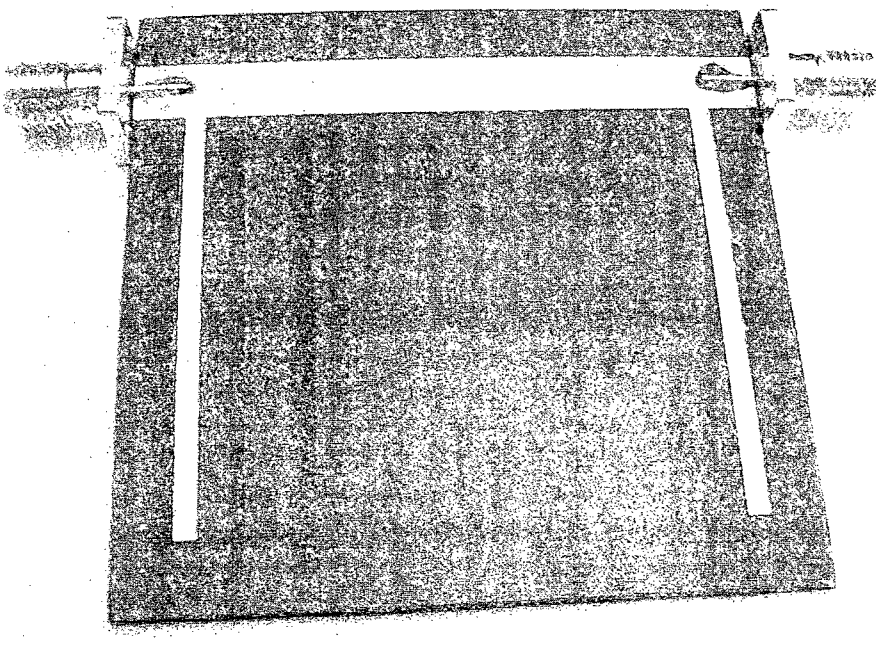

Figure 5.4 BSF Prototype (f_c = 1350 MHz)

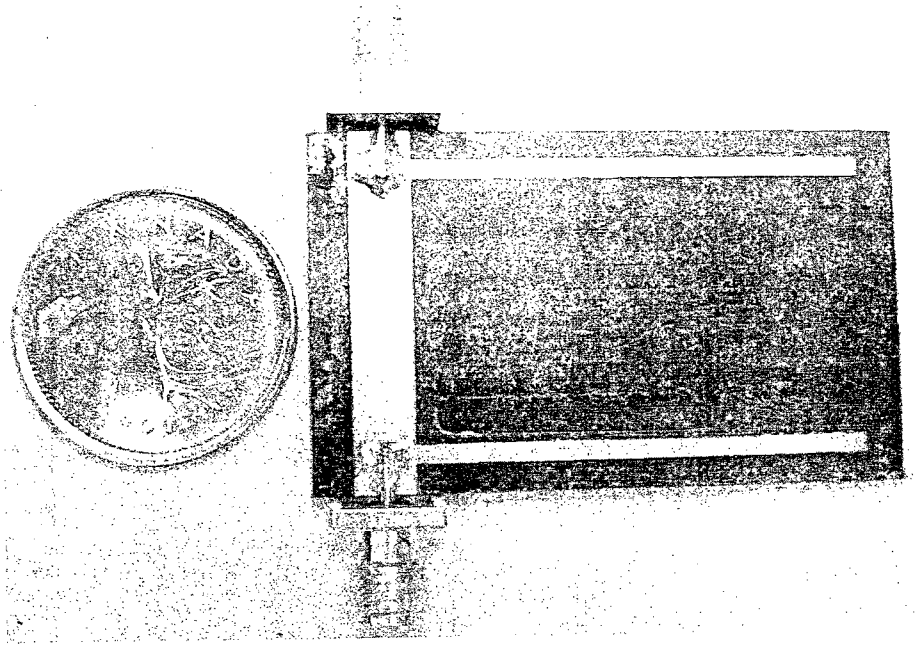

Figure 5.5 BSF Prototype (f_c = 1464 MHz)

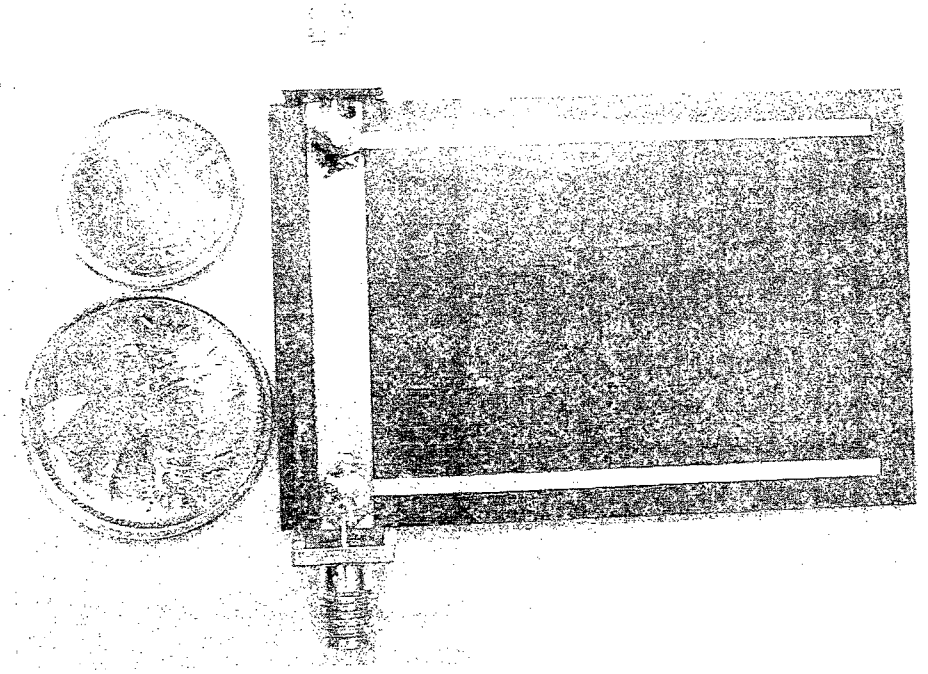

Figure 5.6 BSF Prototype (f_c = 1930 MHz)

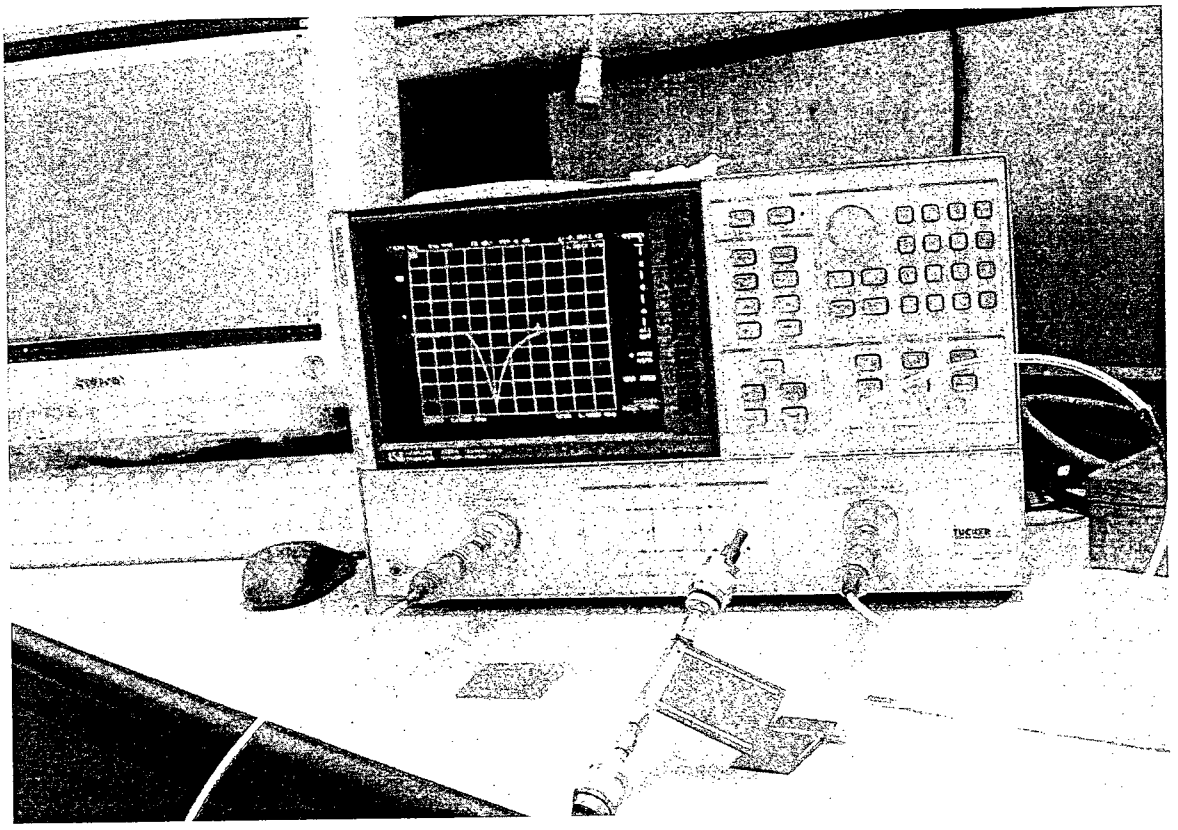

Figure 5.7 BSF Prototype Measured by the HP 8720A Network Analyzer

The measured S-parameters and the phase responses have been tabulated and plotted in the next section. Next, the measured results will then be analyzed and compared against the theoretical ones.

5.2 Measured S-Parameters

In this section, the S-parameters of the BSFs have been measured and tabulated using the HP 8720A Network Analyzer, LabVIEW software, and Microsoft Excel. Figures 5.8 - 5.13 illustrate the S_{11} and S_{21} parameters of each BSF with the peak value of frequency selectivity and the cutoff frequencies.

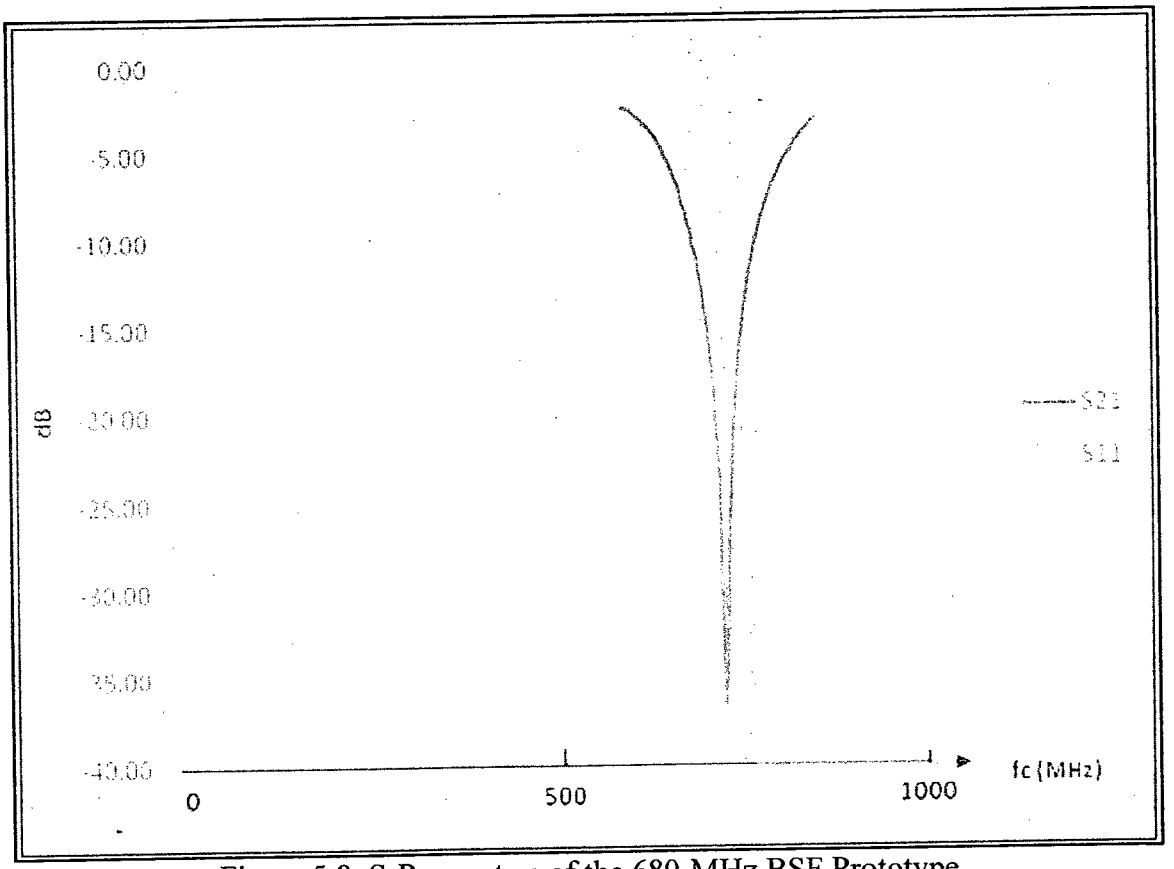

Figure 5.8 S-Parameters of the 680-MHz BSF Prototype

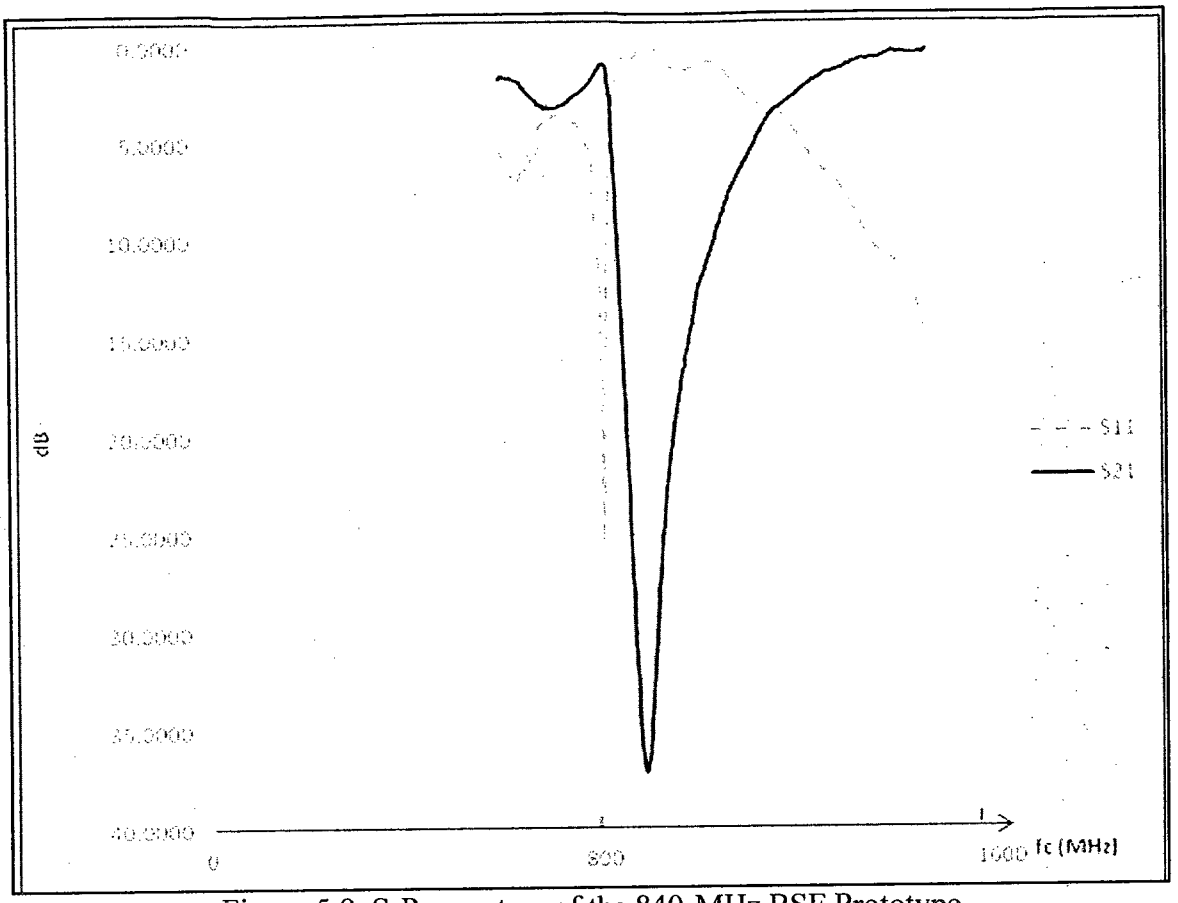

Figure 5.9 S-Parameters of the 840-MHz BSF Prototype

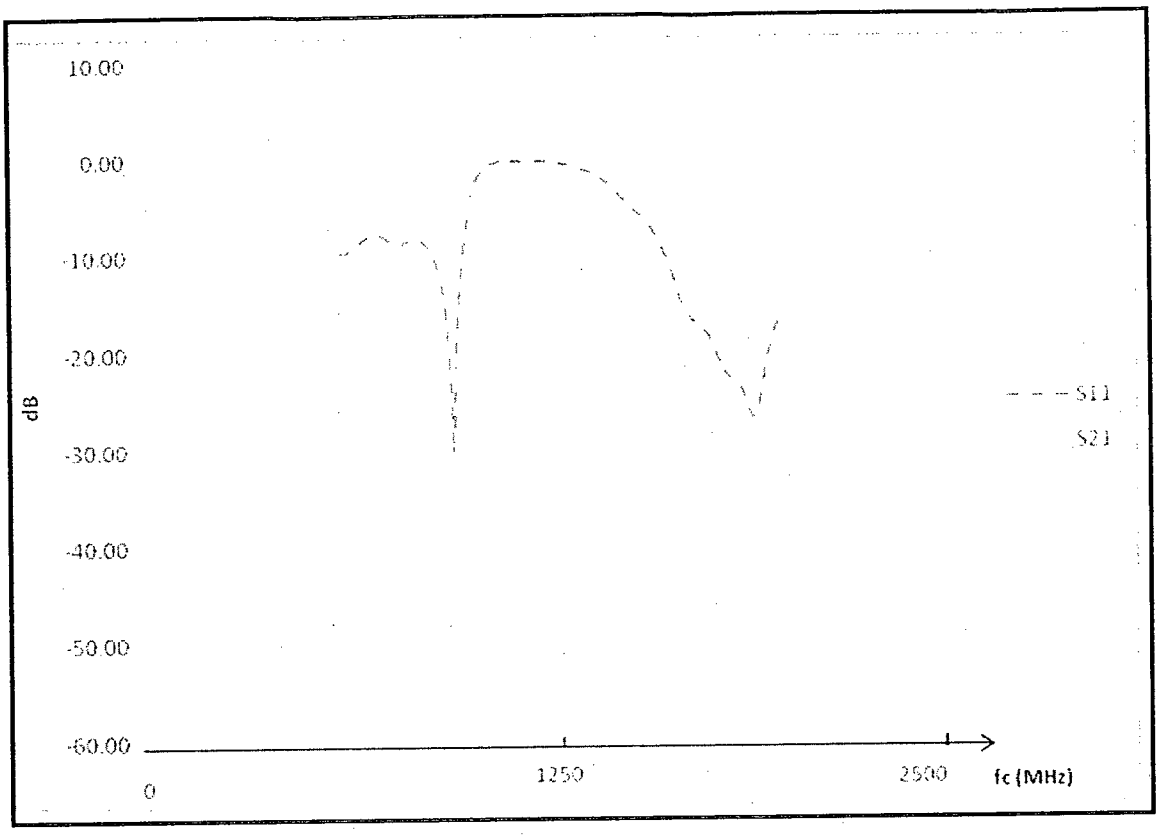

Figure 5.10 S-Parameters of the 1080-MHz BSF Prototype

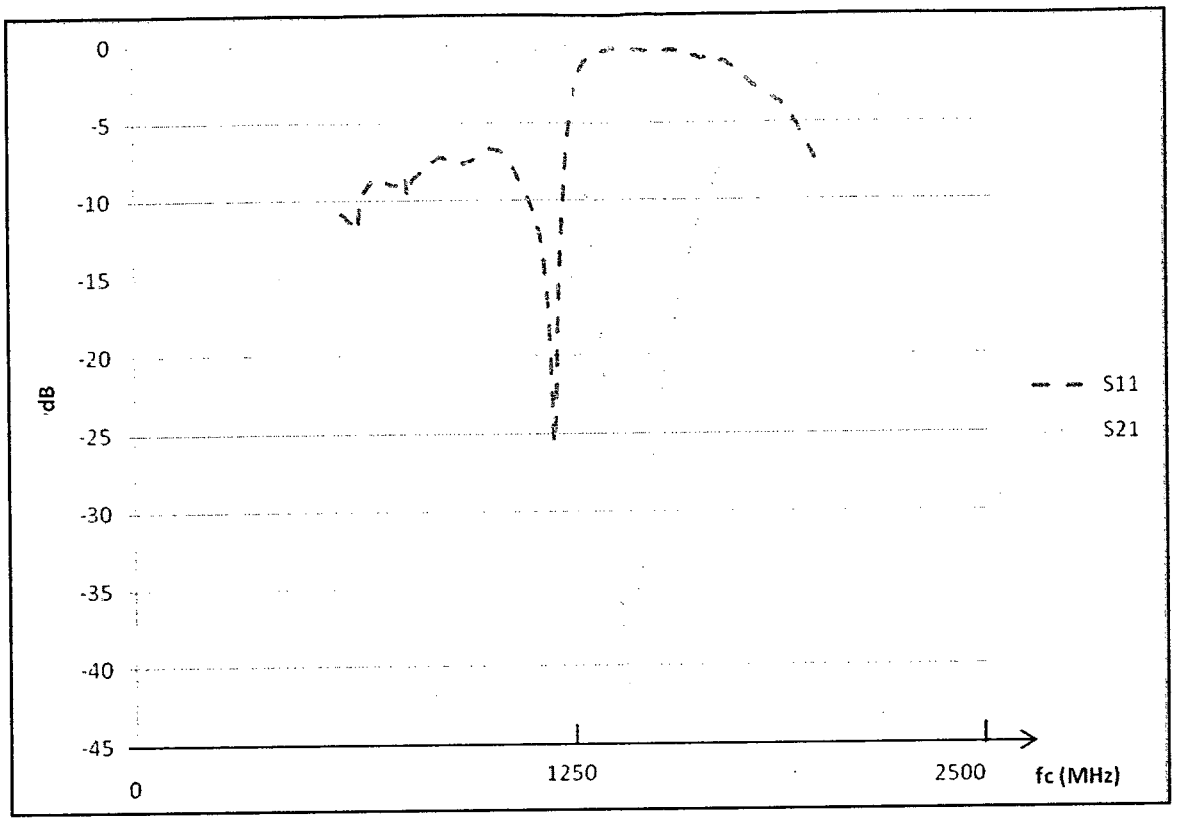

Figure 5.11 S-Parameters of the 1350-MHz BSF Prototype

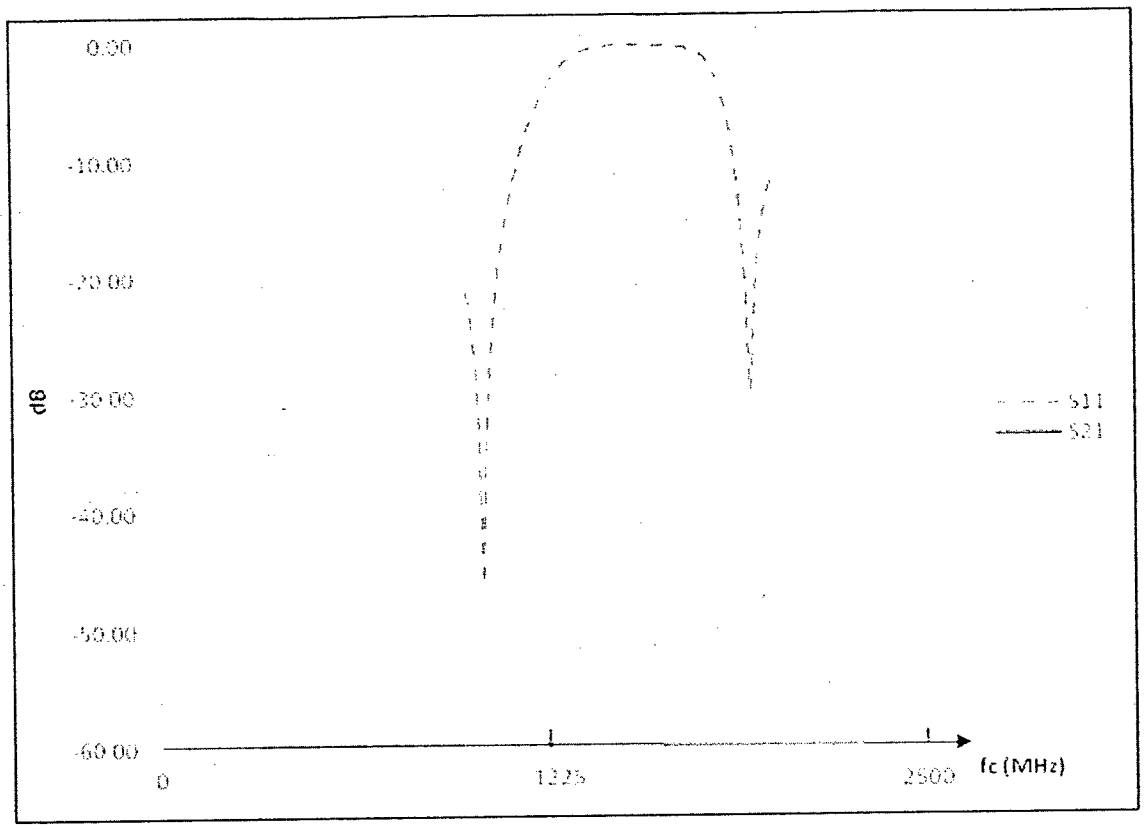

Figure 5.12 S-Parameters of the 1464-MHz BSF Prototype

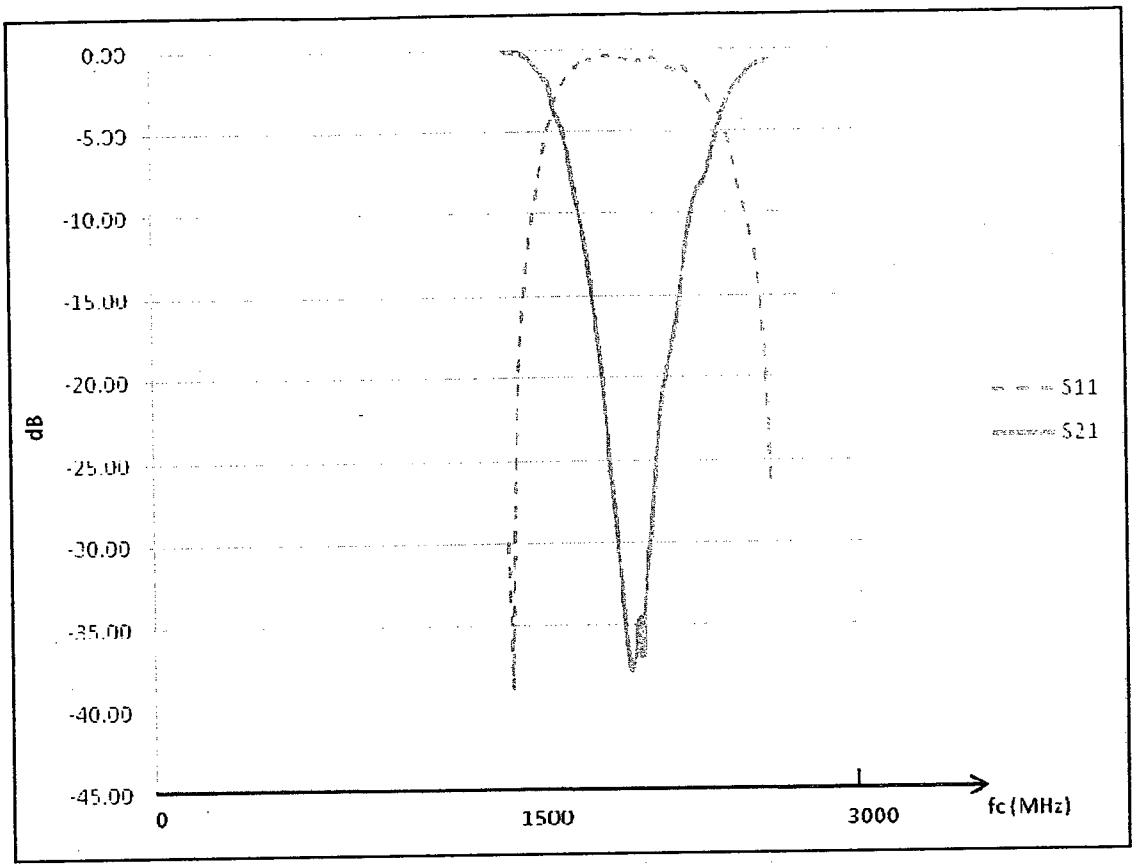

Figure 5.13 S-Parameters of the 1930-MHz BSF Prototype

The next section will focus on the phase responses of the BSF prototypes, corresponding to both S_{11} and S_{21} at each frequency.

5.3 Measured Phase Responses

In this section, the phase responses of the manufactured BSF prototypes have been measured using the same exact frequency sweep used in the previous section. Figures 5.14 – 5.19 illustrate the phase-changes of the BSF prototypes at both S_{11} and S_{21}, measured at the same frequency range as section 5.2.

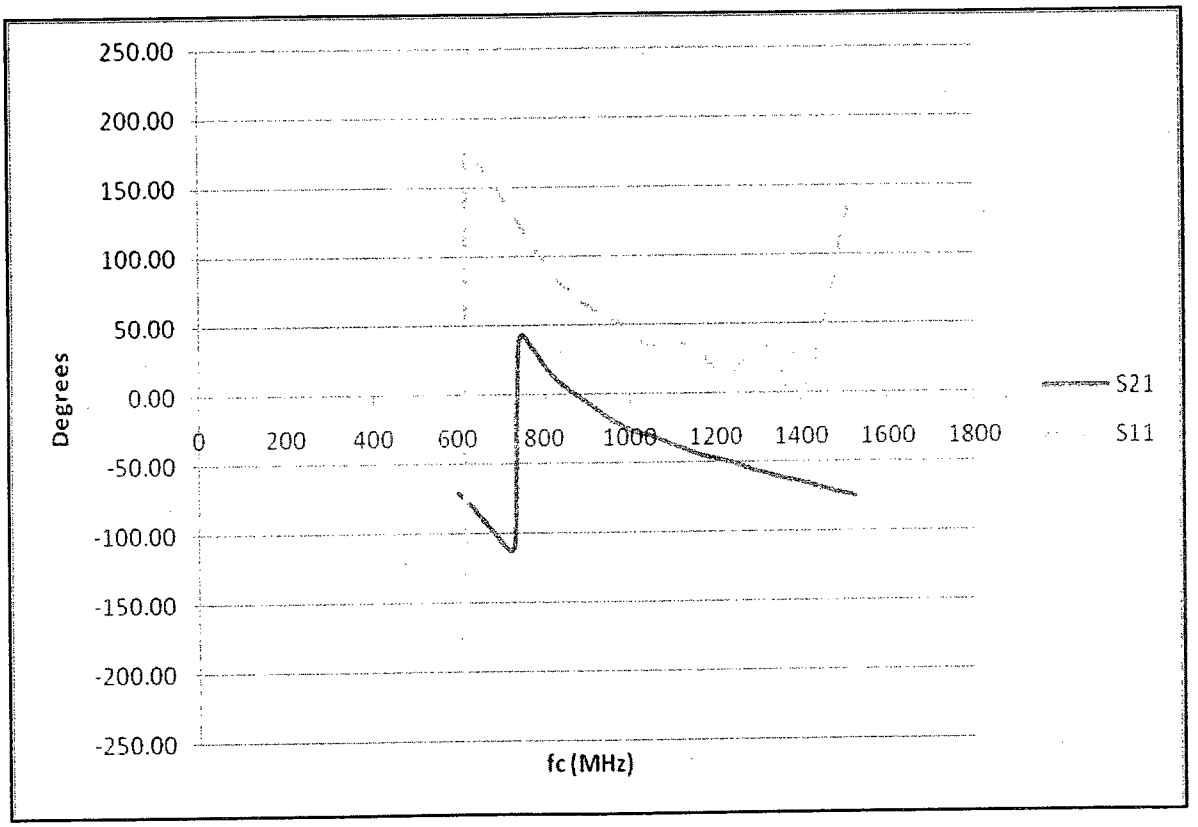

Figure 5.14 Phase Responses of the 680-MHz BSF Prototype

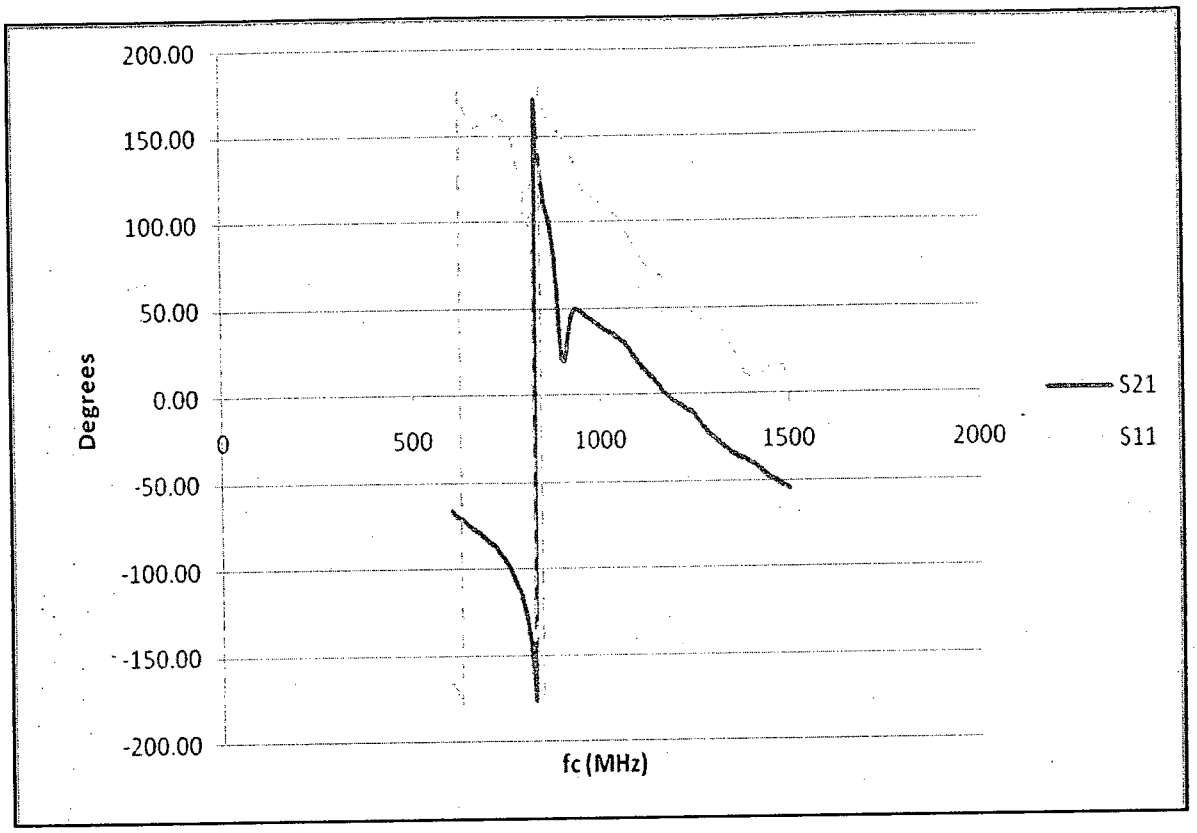

Figure 5.15 Phase Responses of the 840-MHz BSF Prototype

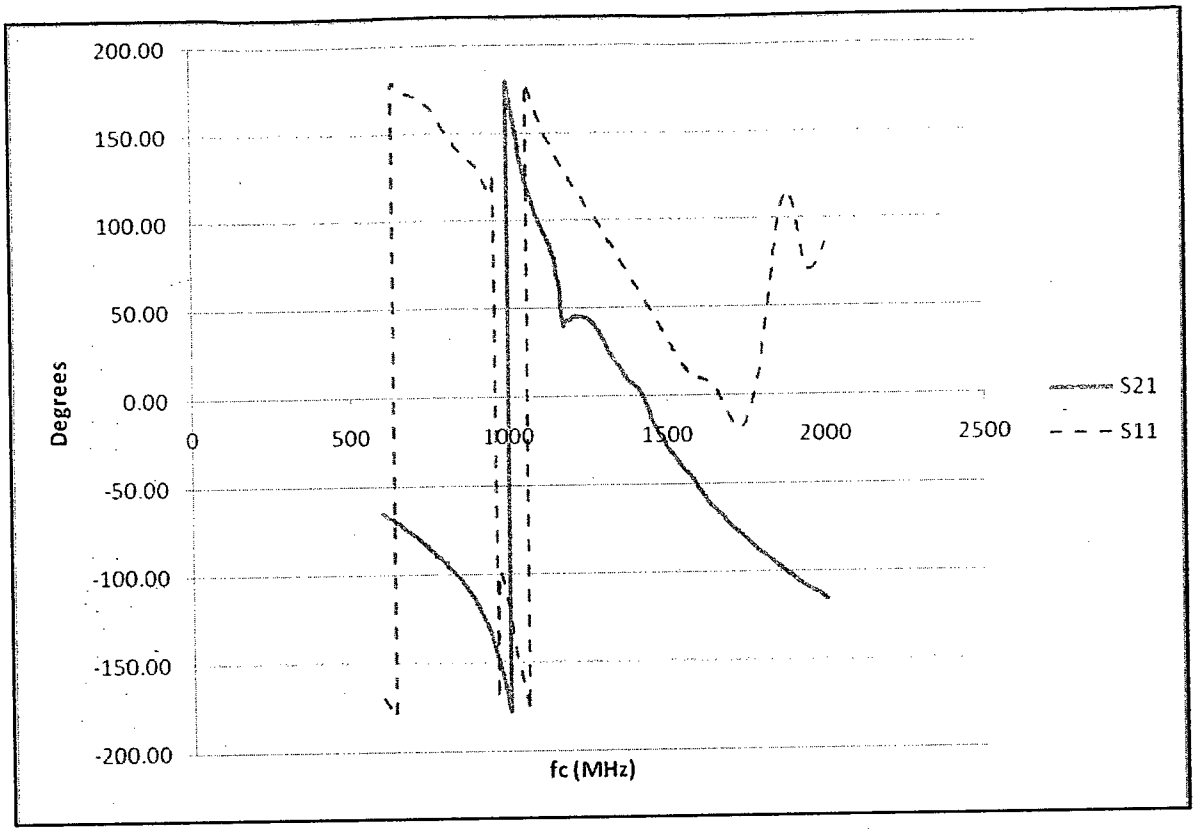

Figure 5.16 Phase Responses of the 1080-MHz BSF Prototype

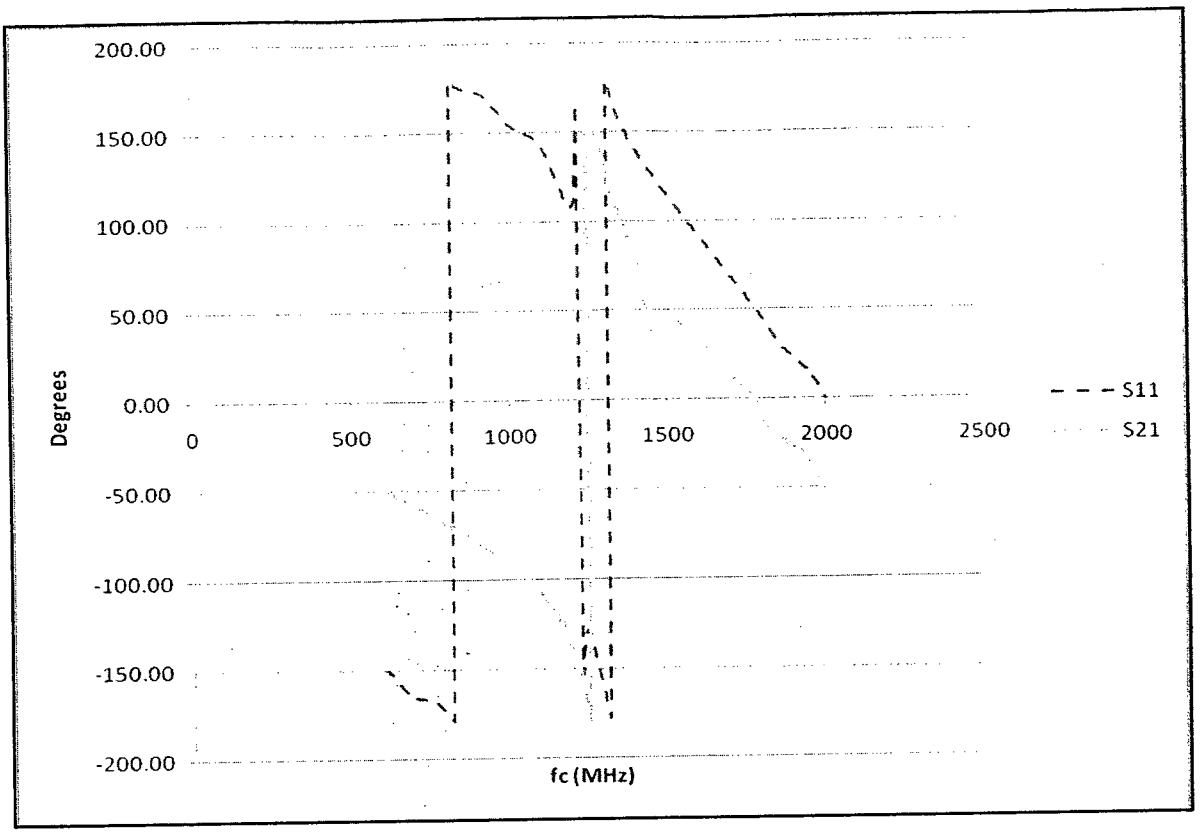

Figure 5.17 Phase Responses of the 1350-MHz BSF Prototype

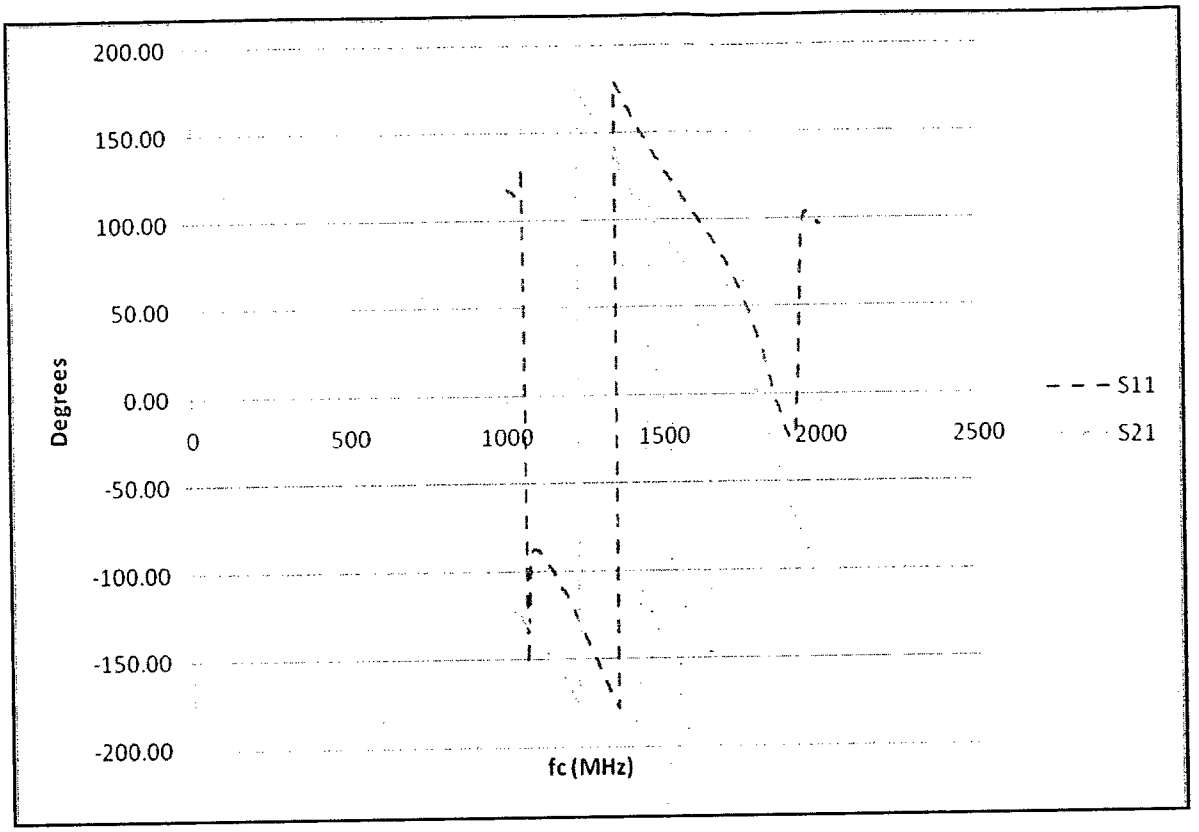

Figure 5.18 Phase Responses of the 1464-MHz BSF Prototype

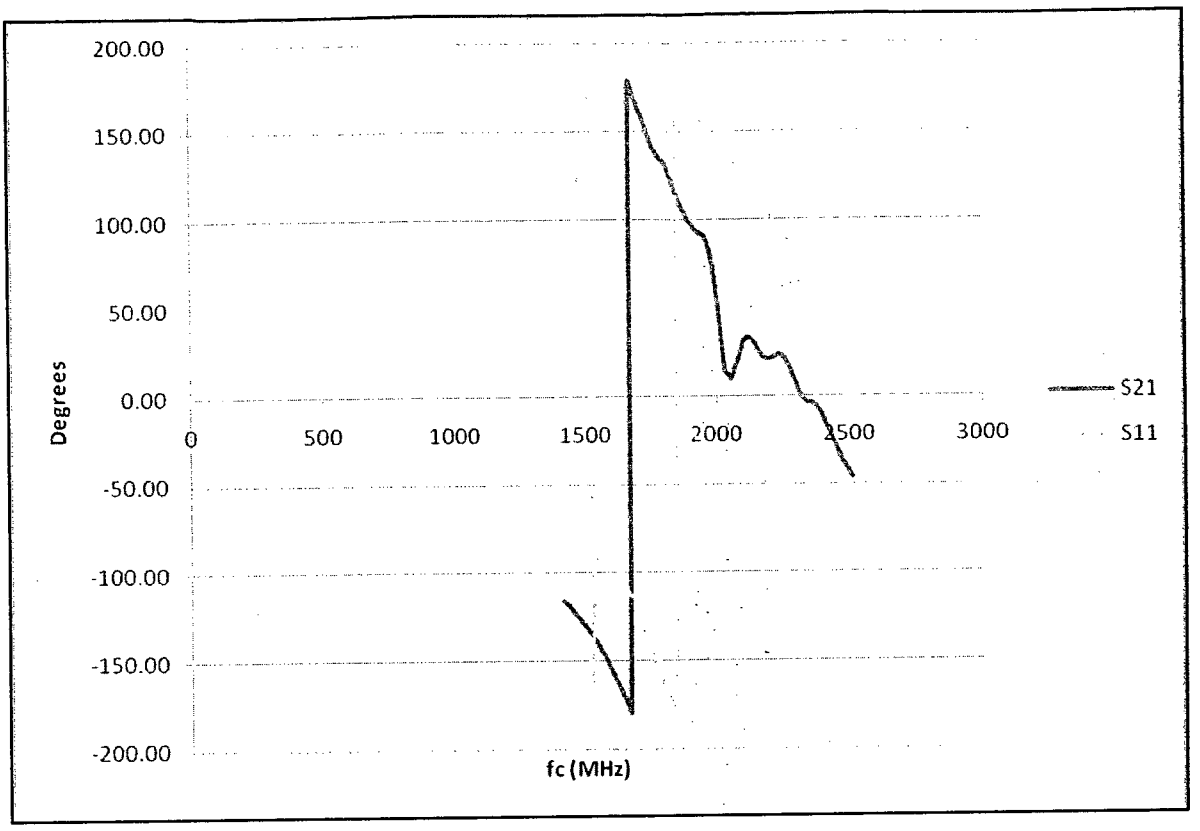

Figure 5.19 Phase Responses of the 1930-MHz BSF Prototype

5.4 Discussion of the Measured Results

5.4.1 The S-Parameters

It is important to note the slight decrease in the selectivity values at cutoff frequencies of the fabricated BSF prototypes, due to the losses in the solder pads, the loss in joints between the connectors and the circuit traces, and the loss in the cables connecting the HP 8720A Network Analyzer to the BSFs. Despite the difference in the selectivity values of the theoretical and measured results, these BSF prototypes will still suppressing great deal of EMI noise, and enhance the Signal to Noise Ratio (SNR) at the wireless receivers

used for the robotic controllers. The BSF design objective of having selectivity of -20 dB or better at the cutoff frequencies has been successfully accomplished.

5.4.2 The Phase Responses

The illustrated phase shifts of Figures 5.14 – 5.19 are well within the expected theoretical values. The phase values near the cutoff frequencies, as well as the perfect shift of the frequency response from the S_{11} to the S_{21} values represent the prompt operation of the filters and their behavior in the tested frequency range of 600-2000 MHz. The occasional ripples observed in the phase responses at S_{21} are due to the occasional movement of the cables during the tests, the imperfections of the filter traces, and the losses introduced to the connectors by somewhat excessive solder pads.

5.5 Summary of Chapter 5

The BSF prototypes have been realized using microstrip traces machine-milled on high-frequency Rogers RT/duroid® 5880 laminates. The prototypes with cutoff frequencies of 680 MHz and beyond have been considered due to smaller sizes and their relevance to the wireless communication spectrum. Both the S-parameters and phases (at S_{11} and S_{21}) have been measured for all the machine-milled BSFs using the HP 8720A Network Analyzer.

The obtained S-parameter plots showed overall satisfactory results, except for slight decreases in frequency selectivity values. Nevertheless, the peak selectivity values at the cutoff frequencies were lower than -20 dB, which satisfied the design objectives.

The phase responses of all the built BSFs were also measured, where the responses at S_{11} and S_{21} showed logical shift with minor ripples due to very sensitive measurement cables and the losses due to circuit trace imperfections.

Chapter 6

Conclusions and Future Work

6.1 Conclusions

This research project has contributed to the radiated EMI level measurements of a medium-size aerospace manufacturing factory floor. As explained in Chapter 3, the radiated EMI levels in the vicinity of robotic and other high-voltage equipment have been conducted and tabulated. Since the focus of this work is on the wireless robotic control and the adverse effects of EMI on it, the measured radiated EMI levels near an operating robotic controller have been considered. The measured EMI levels at each frequency have been compared against the governed limits set by the FCC for Class A industrial equipment. Finally, the problematic frequencies have been identified and form the basis for the filter design tasks of the next chapter. In Chapter 4, the theoretical aspects of microwave BSF design have first been demonstrated. The process of conceptual filter design started with MATLAB. Later on, more accurate prototypes have been finalized and simulated via Ansoft Designer. The Ansoft Designer's capability of producing Gerber files for filter fabrication has provided the opportunity to build the designed BSFs.

In Chapter 5, the BSF prototypes have been realized on Rogers RT/duroid® 5880 high-frequency laminates using machine milling. As a proof of concept, the prototypes have been tested and measured for their S-parameters and their phases. The results have shown

frequency selectivity values of lower than -20 dB at the cutoff frequencies. Although the selectivity values are slightly higher than the theoretical ones due to manufacturing and equipment imperfections, using these filters will significantly reduce the effects of EMI on the wireless robotic controller link. Moreover, the SNR at the robotic controller receiver will be enhanced by the means of suppressing unwanted EMI.

6.2 Recommendations for Future Work

The future recommendations start with perfect electromagnetic shielding of the filters. Adverse effects of radiated EMI and voltage surges of the controller could negatively affect the performance of the filters. Moreover, the effects of the built BSFs on the measured EMI noise are to be simulated using MATLAB, where the outputs of the simulated block set will represent each BSF's behavior and selectivity.

Next, the filters must be fine-tuned and tested for various wireless control commands, since simpler commands (e.g., interfacing or manipulator coordinates position request) require different frequency bandwidth than more complex commands (e.g., arc welding or high-speed intelligent peen forming).

Finally, a perfect matching between the connectors of the BSFs and the wireless modem's antenna and casing is necessary in order to ensure zero signal reflection and to avoid any performance degradation.

References

[1] C.R. Paul, *Introduction to Electromagnetic Compatibility, 2 ed.*, Hoboken, New Jersey, USA: Wiley-Interscience, 2006.

[2] S. Wakamatsu, F. Tilley, G. Hubers, Y. Sakamoto, T. Kaneko, H. Yamamoto, and Y. Karokawa, "To reinforce immunities around GHz frequencies by EMI noise suppression filters," *IEEE Sympo. EMC*, Santa Clara, California, USA, pp. 511 – 514, Aug. 1996.

[3] D.A. Weston, *Electromagnetic Compatibility: Principles and Applications*, New York, U.S.A: Marcel Dekker, 1991.

[4] S. Loyka, "EMC/EMI Analysis in Wireless Communication Networks," *Proc. IEEE Symp. EMC*, Montreal, Canada, vol. 1, pp. 100-105, August 2001.

[5] S. Loyka, "Nonlinear EMI Simulation of an AM Detector at the System Level," *IEEE Trans. EMC*, vol. 42, no. 1, pp.97-102, 2000.

[6] A.H. van Roermund et al., *Analog Circuit Design*, Maastricht, Netherlands: Springer Netherlands, 2006.

[7] D. Masotti, "Computer-aided optimization of broadband nonlinear microwave integrated circuits with the aid of electro-magnetically generated look-up tables," *Microwave Opt. Tech. Letter*, vol. 15, pp. 189-196, 1997.

[8] L. Hsieh, K. Chang, "Compact, Low Insertion-Loss, Sharp-Rejection, and Wide-Band Microstrip Band pass Filters," *IEEE Trans. Microwave Theory Tech.*, vol. 51, no. 4, pp. 1241-1246, 2003.

[9] S.B. Dehia, M. Ramdani, and E. Sicard, *Electromagnetic Compatibility of Integrated Circuits*, Toulouse, France: Springer, 2006.

[10] I. Takahashi, A. Ogata, H. Kanazawa, and A. Hiruma, "Active EMI Filter for Switching Noise of High Frequency Inverters," *Proc. IEEE Conf. Power Conversion* , vol. 1, pp. 331-334, Nagaoka, Aug. 1997.

[11] S. Qu and D. Chen, "Mixed-Mode EMI Noise and Its Implications to Filter Design in Offline Switching Power Supplies," *IEEE Trans. Power Electronics,* vol. 17, no. 4, pp. 502-507, 2002.

[12] G. A. Latheef, S. Karunakaran, and K. Sridhaf, "Tuned band reject power line EMI filter," *Proc. IEEE Conf. EMC*, Santa Clara Valley, USA, pp. 436-439, Aug. 1995.

[13] R. Schmidtt, *Electromagnetic Explained: A Handbook for Wireless / RF, EMC, and High-Speed Electronics*, New Jersey: Elsevier, 2002.

[14] A. Williams and F. Taylor, *Electronic Filter Design Handbook, 4 ed.*, New York, USA: McGraw-Hill, 2006.

[15] D.M. Pozar, *Microwave and RF Design of Wireless Systems*, New York, USA: Wiley, 2001.

[16] Ansoft High Frequency Structure Simulator (HFSS) v.10.0, Ansoft Corp., 225 West Station Square Drive, Pittsburg, PA 15219, USA.

[17] Agilent Advanced Designed Systems (ADS), Agilent Technologies, 1400 Fountaingrove Parkway, Santa Rosa, CA 95403-1799, USA.

[18] S. Wakamatsu, F. Tilley, G. Hubers, Y. Sakamoto, T. Kaneko, H. Yamamoto, and Y. Karokawa, "To Reinforce Immunities Around GHz Frequencies by EMI Noise Suppression Filters," *IEEE Symp. EMC*, Santa Clara, California, USA, pp. 511 – 514, Aug. 1996.

[19] K.C. Gupta, R. Garg, I. Bahl, P. Bhartia, *Microstrip Lines and Slotlines, 2 Ed.*, Massachusetts: Artech House, 1996.

[20] J.S. Hong and M.J. Lancaster, *Microstrip Filters for RF/Microwave Applications*, New York, USA: Wiley-Interscience Publication, 2001.

[21] P. Russer, *Electromagnetics, Microwave Circuit and Antenna Design for Communications Engineering, 2 Ed.*, Norwood, Massachusetts, USA: Artech House, 2006.

[22] K. Chang, I. Bahl, and V. Nair, *RF and Microwave Circuit and Component Design for Wireless Systems*, New York: Wiley-Interscience, 2002.

[23] http://www.metexcorp.com/emirfi_theory.htm

[24] R. Zadeh, I. Mantegh, and C. Perron, "Wireless Communications for Robotic Applications in Manufacturing Environment," *Proc. 10th IASTED Conf. Control and Applications,* Quebec City, Quebec, Canada, May 2008.

[25] E.M. Saenz, G. Subramanyam, F.W. Van Keuls, C. Chen, and F.A. Miranda, "Fixed-Frequency and Frequency-Agile (Au, HTS) Microstrip Bandstop Filters for L-Band Applications," *IEEE Trans. Applied Superconductivity*, vol. 11, no. 1, pp. 395-398, 2001.

[26] MATrix LABoratory (MATLAB) 7.9, The MathWorks Corporation, 3 Apple Hill Drive, Natick, MA 01760-2098, USA.

[27] N. Arbabi, "New CAD Models for Spiral Inductors and EM Coupling for EM Based Circuit Design", *Master of Applied Science Thesis*, Concordia University, Montreal, Canada, July 2008.

[28] A.N. Zainal Abidin, W.R Wan Abdullah, N. Hashim, and A. Ramli, "The Effect of Common and Differential Mode Noise on VCC and Ground towards Overall Radiated Emission performances," *Proc. ICEEI 2007*, Bandung, Indonesia, pp. 230-233, June 2007.

[29] http://focus.ti.com/lit/an/slla057/slla057.pdf

[30] S.N. Uysal, "A compact coplanar stripline lowpass filter," *Asia Pacific Microwave Conf. Dig.*, Singapore, vol. 2, pp. 307-310, Nov.-Dec. 1999.

[31] P.A. Rizzi, *Microwave Engineering Passive Circuits*, Englewood Cliffs, New Jersey, USA: Prentice Hall, 1988.

[32] D.R. Jachowski, "Passive Enhancement of Resonator Q in Microwave Notch Filters," *IEEE MTT-S International*, vol. 3, pp. 1315-1318, June 2004.

[33] R.J. Cameron, C.M. Kudsia, and R.R. Mansour, *Microwave Filters for Communication Systems: Fundamentals, design, and Applications*, Hoboken, New Jersey, USA: Wiley-Interscience, 2007.

[34] S. Y. Huang and Y. H. Lee, "A Tapered Small-Size EBG Microstrip Bandstop Filter Design with Triple EBG Structures," IEEE Microwave Opt. Tech. Letters, vol. 46, no. 2, pp. 154-158, 2005.

[35] J. Randa, D. Gilliland, W. Gjertson, W. Lauber, and M. McInerney, "Catalogue of Electromagnetic Environment Measurements, 30-300 MHz," *IEEE Trans. EMC*, vol. 37, no. 1, pp. 26-33, 1995.

[36] D. Middleton, "Statistical-Physical Models of Electromagnetic Interference," *IEEE Trans. EMC*, vol. 19, no. 3, pp. 106-127, 1977.